

Metallicity of RR Lyrae stars from the *Gaia* Data Release 3 catalogue computed with Machine Learning algorithms.

Tatiana Muraveva^{1*}, Andrea Giannetti², Gisella Clementini¹, Alessia Garofalo¹ and Lorenzo Monti¹

¹ *INAF - Osservatorio di Astrofisica e Scienza dello Spazio di Bologna, Via Piero Gobetti 93/3, Bologna 40129, Italy*

² *Istituto di Radioastronomia - INAF, Via Piero Gobetti 101, Bologna 40129, Italy*

Accepted XXX. Received YYY; in original form ZZZ

ABSTRACT

We present new $P - \phi_{31} - [\text{Fe}/\text{H}]$ and $P - \phi_{31} - A_2 - [\text{Fe}/\text{H}]$ relations for fundamental-mode (RRab) and first-overtone mode (RRc) RR Lyrae stars (RRLs), respectively. The relations were calibrated based on pulsation periods and Fourier parameters of the RRL light curves in the *Gaia* *G*-band published in the *Gaia* Data Release 3 (DR3), and accurate spectroscopically measured metallicities available in the literature. We apply the feature selection algorithm to identify the most relevant parameters for the determination of metallicity. To fit the relations, we used the Bayesian approach, which allowed us to carefully take into account uncertainties in various parameters and the intrinsic scatter of the relations. The root mean squared errors of the predicted metallicity values in the training samples are 0.28 dex and 0.21 dex for RRab and RRc stars, respectively, comparable with the typical uncertainty of low/intermediate resolution spectroscopic metallicity measurements. We applied the new relations to measure individual metallicities and distances to $\sim 134,000$ RRLs from the *Gaia* DR3 catalogue, as well as mean metallicities and distances to 38 Milky Way globular clusters. We also estimate the mean metallicity and distance to the Large Magellanic Cloud (LMC) and Small Magellanic Cloud (SMC): $[\text{Fe}/\text{H}]_{\text{LMC}} = -1.63 \pm 0.36$ and $\mu_{\text{LMC}} = 18.55 \pm 0.18$ mag, $[\text{Fe}/\text{H}]_{\text{SMC}} = -1.86 \pm 0.36$ dex and $\mu_{\text{SMC}} = 19.01 \pm 0.17$ mag, respectively, in excellent agreement with previous measurements.

Key words: stars: variables: RR Lyrae – stars: abundances – Magellanic Clouds – methods: data analysis

1 INTRODUCTION

RR Lyrae (RRLs) are pulsating variable stars that play a crucial role in stellar astrophysics. They are low-mass ($M < M_{\odot}$), old (age > 10 Gyr) stellar objects that populate the classical instability strip region of the horizontal branch (HB) in the colour–magnitude diagram (CMD). RRLs exhibit periodic variations in luminosity from about 0.2 mag up to more than a one magnitude in the visual band, occurring over a timescale ranging from a few hours to one day, which makes them easily detectable. They can be divided into three classes based on the pulsation modes: fundamental mode (RRab), first-overtone (RRc) and pulsating in both modes (RRd) stars. RRLs are abundant in the Milky Way (MW) halo and specific stellar systems, such as globular clusters (GCs), dwarf spheroidal (dSph) galaxies, and ultra-faint dwarf (UFD) galaxies, and are extensively used to study the properties of their host stellar systems (e.g. Sesar et al. 2014, Molnár et al. 2015, Muraveva et al. 2020, Garofalo et al. 2021). The presence of numerous RRLs in the MW halo provides an excellent opportunity to investigate the halo’s overall shape, map the halo’s substructures and constraint models of the formation and evolution of our Galaxy (e.g. Drake et al. 2013, Belokurov et al. 2018, Iorio & Belokurov 2019, 2021).

RRLs are unique objects because their intrinsic properties, such

as distance and metallicity ($[\text{Fe}/\text{H}]$), can be determined from easily observed photometric parameters (apparent magnitude, pulsation period, etc.). It is well known that one of the most direct and reliable methods to measure distance is trigonometric parallax, the determination of which requires accurate astrometric observations. The European Space Agency mission *Gaia* (Gaia Collaboration et al. 2016) recently provided parallaxes for an unprecedented number of stars. However, the accuracy of the *Gaia* Early Data Release 3 (EDR3) parallaxes (0.02–0.03 mas for $G < 15$ mag) drops dramatically for fainter objects, reaching values of 1.3 mas at $G = 21$ mag (Gaia Collaboration et al. 2021), which hampers a reliable estimation of distances directly from parallaxes for farther objects. Fortunately, RRLs can serve as reliable distance indicators helping to overcome *Gaia*’s limits. In fact, the distance to RRLs can be determined using the absolute magnitude–metallicity relation in the visual band ($M_V - [\text{Fe}/\text{H}]$, e.g. Clementini et al. 2003, Bono et al. 2003), near-/mid-infrared period–luminosity–metallicity (*PLZ*) relations (e.g. Longmore et al. 1986, Sollima et al. 2008, Madore et al. 2013, Muraveva et al. 2018b,c) and fundamental relations calibrated directly in the *Gaia* *G*, *G_{BP}* and *G_{RP}* bands (e.g. Muraveva et al. 2018c, Garofalo et al. 2022, Li et al. 2023).

At the same time, RRLs serve as useful metallicity tracers. The most direct method of measuring RRL metal abundances is from high-resolution (HR, $R \geq 20,000$) spectra, which provide metallicities with an accuracy of ~ 0.1 dex but require a large amount of

* E-mail: tatiana.muraveva@inaf.it

telescope time. Nowadays, the metallicities measured from HR spectra exist for only a few hundred RRLs (e.g. [Clementini et al. 1995](#), [Lambert et al. 1996](#), [For et al. 2011](#), [Nemec et al. 2013](#), [Pancino et al. 2015](#), [Chadid et al. 2017](#)), even though this number increased significantly in the last few years ([Crestani et al. 2021](#), [Gilligan et al. 2021](#)). The metallicity of RRLs can also be determined from low-resolution (LR) spectra through the ΔS method ([Preston 1959](#)), which relies on the ratio between the equivalent width of Ca and H lines. The application of this method increases the number of RRLs with available metallicities to thousands (e.g. [Liu et al. 2020](#), [Crestani et al. 2021](#)), but it is less accurate (typical error of $\sim 0.2 - 0.3$ dex) and requires intermediate calibrations, which can introduce additional systematic errors.

Fortunately, the metallicities of RRLs can also be determined using solely photometric observations. [Jurcsik & Kovacs \(1996\)](#) found a linear relation between the metallicity of RRab stars and the Fourier parameter ϕ_{31} of their light curves in the V band, along with the pulsation period. Later [Morgan et al. \(2007\)](#) produced a similar relation for RRc stars. Several authors calibrated these relations in other passbands (e.g. [Smolec 2005](#), [Nemec et al. 2013](#), [Mullen et al. 2021](#)). [Hajdu et al. \(2018\)](#) adopted a different approach to the problem of metallicity prediction, applying Machine Learning (ML) algorithms to the K_s -band light curves. Recently [Dékány et al. \(2021\)](#) used ML methods to derive the relation between Fourier parameters of the RRL light curves in the I -band, period and metallicity based on a sample of stars with metallicity known from HR spectroscopy.

Nowadays, it is a unique moment for RRLs thanks to data from large surveys, such as *Gaia* ([Gaia Collaboration et al. 2016](#)). *Gaia*'s latest Data Release 3 (DR3) has provided the largest, most homogeneous and parameter-rich catalogue of RRLs ever published ([Clementini et al. 2023](#)). Thus, calibration of the RRLs photometric metallicities directly from the G -band light curves becomes timely, especially in light of the coming *Gaia* DR4. To the best of our knowledge, direct relations between parameters of the RRL G -band light curves and metallicity were provided so far by [Iorio & Belokurov \(2021\)](#), who used *Gaia* DR2 data and LR-spectroscopic metallicities from [Layden \(1994\)](#), and by [Li et al. \(2023\)](#), who used *Gaia* DR3 light curves and a sample of RRLs with LR spectroscopy measurements from [Liu et al. \(2020\)](#). At the same time, [Dékány & Grebel \(2022\)](#) used recurrent neural networks to predict the metallicity of RRLs from their K_s and *Gaia* DR2 G -band light curves.

In this paper, we derive new relations between periods, the Fourier parameters of the G -band light curve of RRLs and metallicity based on data from *Gaia* DR3 and HR/LR spectroscopic metal abundances available in the literature. To produce the new relations, we perform an accurate feature selection procedure and apply the Bayesian approach, allowing us to take into account possible systematics and properly estimate errors. We then apply our new relations to measure the photometric metallicities of 134,769 RRLs from the *Gaia* DR3 catalogue ([Clementini et al. 2023](#)). These metallicity estimates were used to calculate distances to RRLs applying the G -band luminosity-metallicity ($M_G - [\text{Fe}/\text{H}]$) relation from [Garofalo et al. \(2022\)](#). We analyse the MW structures traced by RRLs and provide new estimates of metallicity and distances to a number of GCs, hosting RRLs, and to the Magellanic Clouds. The paper is structured as follows: Section 2 describes the dataset we used in our study. Section 3 outlines the applied methods. In Section 4, we perform different tests to evaluate the quality of the metallicities obtained in this study. In Section 5, we estimate the distances to RRLs and analyse the MW structures as traced by RRLs. In Section 6 we study RRLs located in the Magellanic Clouds. Finally, Section 7 summarises our main results.

2 DATA

2.1 *Gaia* DR3 sample of RRLs

Gaia DR3 provides a catalogue of 271,779 RRLs observed during the initial 34 months of science operations and processed through the Specific Object Study pipeline for Cepheids and RR Lyrae stars (SOS Cep&RRL, [Clementini et al. 2023](#)). This catalogue includes, among others, information on pulsation periods, peak-to-peak amplitudes of the G , G_{BP} and G_{RP} light curves, classification in pulsation mode, mean magnitudes computed as an intensity-average over the complete pulsation cycle, and parameters of the Fourier decomposition of the G -band light curves. During the final validation of the dataset [Clementini et al. \(2023\)](#) discarded 888 stars, mainly eclipsing binaries and objects with an uncertain classification. Thus, the final *Gaia* DR3 sample contains 270,891 RRLs (174,941 RRab, 93,944 RRc and 2006 RRd stars). We exclude RRd stars from our analysis and then cross-matched the remaining sample against the OGLE IV catalogue ([Soszyński et al. 2014, 2019](#)). There are 100,558 stars in common, for which we compared periods and classifications provided in both surveys. We found that classification in pulsation modes differ for 2505 stars, while there is a discrepancy in periods of more than 0.001 days for other 1520 sources. Since the sampling and temporal baseline of the OGLE light curves are usually better than those of *Gaia*, we decided to discard from our analysis the sources with classifications or periods different from the OGLE catalogue.

The left panel of Figure 1 shows the Bailey (amplitude in the G -band versus pulsation period) diagram for RRab (red dots) and RRc (blue dots) stars in the remaining sample of 264,860 RRLs. As can be seen, some stars classified as RRab are situated within the zone typically occupied by RRc stars. These could be RRc stars misclassified as RRab stars or RRd stars with less than 40 transits observed by *Gaia*, for which the SOS pipeline does not search for the second periodicity ([Clementini et al. 2023](#)). Additionally, some RRab and RRc stars are positioned outside the expected loci, potentially indicating inaccuracies in their classification or periods provided in the *Gaia* DR3 catalogue. We cleaned the sample by selecting only RRLs located in the zones occupied by *Gaia* DR3 RRLs confirmed by OGLE. In order to do this we made a 2D Cartesian cross-match between period and the G -band amplitude of 264,860 RRLs shown in the left panel of Fig. 1 and those parameters for the sample of *Gaia* DR3 RRLs confirmed by OGLE. The right panel of Fig. 1 shows the distribution of the clean sample of 258,696 RRLs (hereafter, GAIA-CAT-RRLS, Table 1) on the Bailey diagram. We used this catalogue as a reference in the following analysis.

2.2 HR spectroscopic dataset

To the best of our knowledge, the most extensive single catalogue of RRLs, for which metallicity is determined from HR spectroscopy, is published by [Crestani et al. \(2021\)](#). Most RRL spectra were collected with the echelle spectrograph at du Pont (Las Campanas Observatory). This dataset was complemented with the HR metallicities estimated by [For et al. \(2011\)](#), [Chadid et al. \(2017\)](#) and [Snedden et al. \(2017\)](#). According to [Crestani et al. \(2021\)](#), their measurements of metallicities, along with estimates from the three mentioned studies, can be treated as a single homogeneous sample, covering the range from -3.0 to 0.2 dex. The final calibrating sample of [Crestani et al. \(2021\)](#) includes 143 RRLs (111 RRab and 32 RRc stars). We used this catalogue as a reference sample for our training set.

[Crestani et al. \(2021\)](#) calculated metallicities based on direct equivalent width measurements of both neutral (FeI) and ionized (FeII)

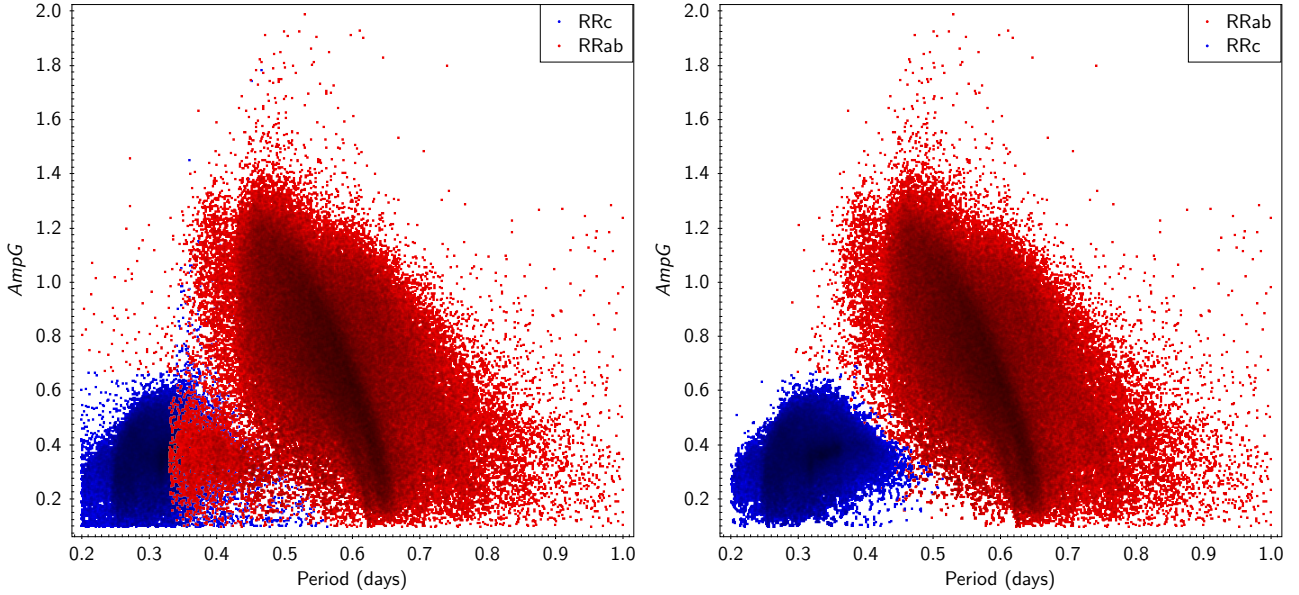


Figure 1. *Left panel:* Bailey diagram for RRab (red dots) and RRC (blue dots) stars in the *Gaia* DR3 catalogue. *Right panel:* Clean sample selected based on the RRLs' location on the Bailey diagram (GAIA-CAT-RRLS). See text for details.

Table 1. Catalogues of RRLs used in the analysis

Name	Source	RRab	RRC	Total	[Fe/H] range RRab (dex)	[Fe/H] range RRC (dex)	Period range RRab (days)	Period range RRC (days)
HR-CAT-RRLS	Crestani et al. (2021), Gilligan et al. (2021)	126	24	150	[-3.06, 0.11]	[-2.60, -0.49]	[0.36, 0.96]	[0.22, 0.41]
LR-CAT-RRLS	Liu et al. (2020)	797	452	1249	[-2.92, -0.10]	[-2.87, -0.32]	[0.36, 0.93]	[0.22, 0.45]
GAIA-CAT-RRLS	Clementini et al. (2023)	169,024	89,672	258,696	-	-	[0.29, 1.00]	[0.20, 0.51]

iron lines in the HR spectra. When more than one measurement was available for a given star, the final metallicity value was calculated as the mean of all measurements, while the uncertainty was computed as the standard deviation of these measurements. However, this approach does not take into account individual uncertainties provided for each measurement. As a result, uncertainties in metallicities provided for some stars (Table 5 in Crestani et al. 2021) reach zero values. It is important to stress that robust uncertainty estimations are crucial for creating an accurate predictive model based on Bayesian analysis (Dékány et al. 2021). Thus, in our analysis, we recalculate the uncertainties of the metallicities provided by Crestani et al. (2021) by calculating the mean value of uncertainty of all available individual metallicity measurements (columns 8 and 10 in their Table 2) and adding it in quadrature to the uncertainty provided by Crestani et al. (2021) (column 4 of their Table 5). For the metallicities calculated by For et al. (2011), Chadid et al. (2017) and Sneden et al. (2017), we adopt 0.15 dex as a mean uncertainty of the individual metallicity measurements. Uncertainties calculated in this way span the range from 0.07 to 0.33 dex with a mean value of 0.17 dex.

Recently, Gilligan et al. (2021) provided metallicities for 49 RRLs measured from HR spectra taken with the Southern African Large Telescope (SALT). The typical uncertainty of their metallicity measurements is 0.15 dex. In order to check if the metallicities determined by Gilligan et al. (2021) and Crestani et al. (2021) are on the same metallicity scale, we compare metal abundances calculated in both studies for 20 RRLs in common (Fig. 2). Apart from two obvious outliers (AU Vir and RW Tra), shown in grey, there is no visible offset between the two sets of metallicity measurements. The reason

of discrepancy between the metallicity measurements for the two outliers is not clear. However, comparison with LR-spectroscopic metallicity estimates from Zinn et al. (2020) confirms the metallicity values provided by Crestani et al. (2021) for these two stars. The weighted mean difference between Crestani et al. (2021) and Gilligan et al. (2021) metallicity measurements for the 20 RRLs in common is 0.05 dex, which is significantly smaller than the individual uncertainties. The difference has a negligible value of -0.005 dex if the two outliers shown in grey are excluded. We can conclude that the HR-spectroscopic metallicity measurements of Crestani et al. (2021) and Gilligan et al. (2021) can be considered to be on the same metallicity scale. Thus, we added 29 additional RRLs from Gilligan et al. (2021) to our sample of RRLs with HR spectroscopy metallicity estimates without applying any additional shift. Our sample of RRL calibrators with metal abundance from HR spectroscopy, thus, comprises 172 stars.

We cross-matched our catalogue of RRLs with HR spectroscopy metal abundance against the GAIA-CAT-RRLS sample (Section 2.1) and found 162 RRLs in common. We compared the periods provided for these stars in the *Gaia* DR3 catalogue and in the literature (Crestani et al. 2021, Gilligan et al. 2021) and found that they differ by more than 0.001 days for seven sources. The light curves of these seven RRLs are shown in Fig. 3, where the periods from the literature were used to fold the data in the left panels and the *Gaia* DR3 periods in the right panels. Based on the visual inspection of the light curves, we confirm the period provided in the *Gaia* DR3 catalogue for the four sources with *Gaia* source_id: 2373827054405627904, 4344296958198114688,

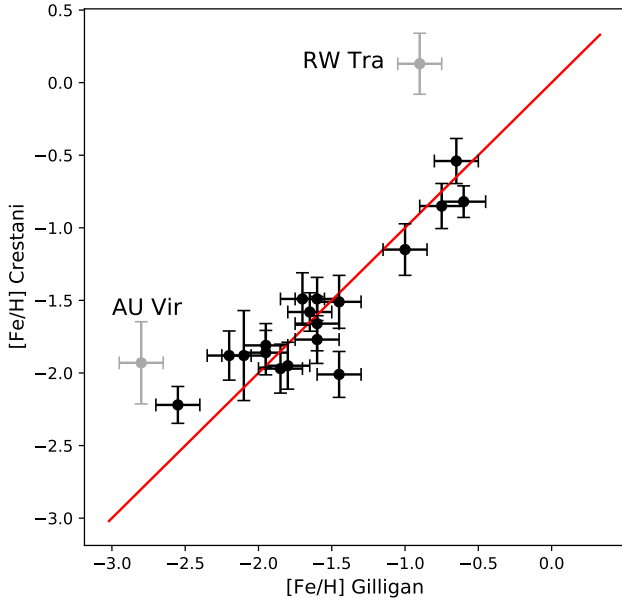


Figure 2. Comparison between metallicities provided by [Crestani et al. \(2021\)](#) and [Gilligan et al. \(2021\)](#) for 20 RRLs in common

5360400630327427072 and 3846786226007324160. For the remaining three stars (2622375506154471680, 6120897123486850944, 6771307454464848768), the periods from the literature are correct (for the latter see also Table A.3 footnote (f) in [Clementini et al. 2023](#)). We exclude the latter three sources from our sample since their periods and, consequently, Fourier parameters provided in the *Gaia* catalogue could be incorrect.

We visually inspected the *G*-band light curves of all RRLs in the HR-spectroscopy sample. We found that nine stars have noisy light curves or gaps close to their light curves' maximum or minimum. Both issues could have affected the accurate estimation of the Fourier parameters of these RRLs; hence, we excluded them from our sample. Thus, our final sample of RRLs with metallicities determined from HR spectroscopy (hereafter, HR-CAT-RRLs) comprises 150 RRLs (Table A1). The metallicity distribution of the RRLs in the HR-CAT-RRLs is shown in the left panel of Fig. 4, while the left panel of Fig. 5 shows their spatial distribution. The HR-CAT-RRLs includes RRLs from the bulge, disk, and halo of the MW. Table 1 contains more details on this sample.

2.3 LR spectroscopic dataset

[Liu et al. \(2020\)](#) published a catalogue of 5290 RRLs with metal abundances from low-resolution spectra of the LAMOST Experiment for Galactic Understanding and Exploration (LEGUE) and the Sloan Extension for Galactic Understanding and Exploration (SEGUE) surveys, estimated using the ΔS index ([Preston 1959](#)). For this study, we selected only sources with spectral signal-to-noise ratio (S/N) larger than 50 from the [Liu et al. \(2020\)](#) sample. We then cross-matched this catalogue against the GAIA-CAT-RRLs sample (see Section 2.1) and found 1249 stars in common. Hereafter, we call this sample of RRLs with the metallicity estimated from LR spectroscopy LR-CAT-RRLs. See Table 1 for more details on this catalogue.

The metallicity distribution of the RRLs stars in the LR-CAT-RRLs sample is shown in the right panel of Fig. 4, while the right

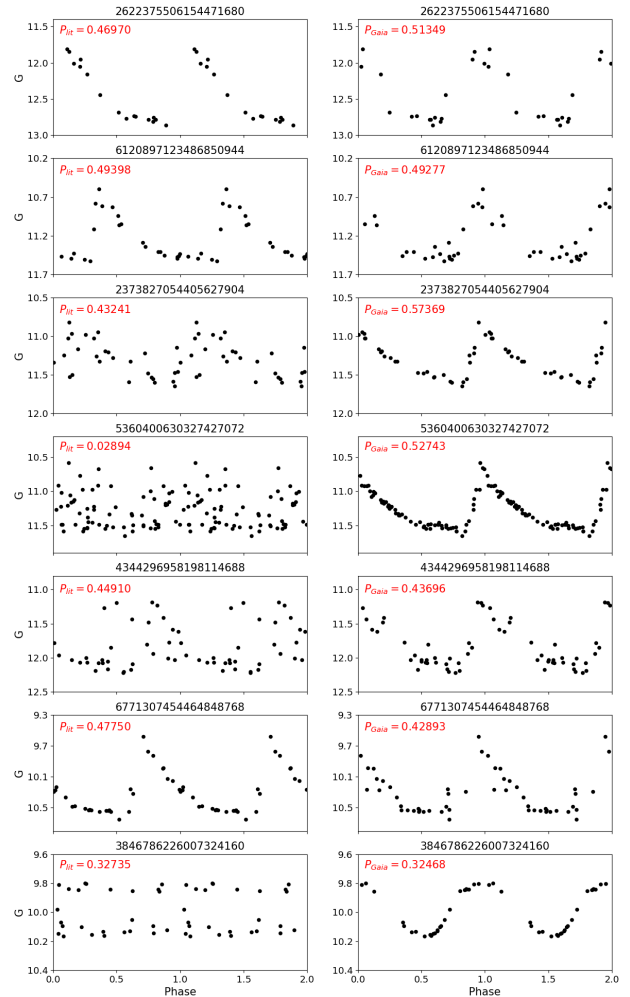


Figure 3. Light curves of sources, for which periods provided in the literature ([Crestani et al. 2021](#), [Gilligan et al. 2021](#)) are in disagreement with those provided in *Gaia* DR3 catalogue. *Left panels:* Light curves phased using periods from the literature. *Right panel:* Light curves phased with the periods from the *Gaia* DR3 catalogue.

panel of Fig. 5 shows their spatial distribution. Fig. 5 shows that RRLs in the HR-CAT-RRLs and LR-CAT-RRLs catalogues are distributed in a somehow complementary way. RRab stars in the HR-CAT-RRLs (Table 1) span a slightly wider metallicity range than RRab stars in the LR-CAT-RRLs sample (Table 1). Metallicity values measured using HR spectroscopy are also more accurate and do not imply intermediate calibrations, which can be an additional source of systematic errors. On the other hand, an important advantage of the LR-CAT-RRLs sample is that it includes many more RRab and, especially, RRc stars compared with the HR-CAT-RRLs sample. In the following analysis, we used the LR-CAT-RRLs sample when statistics over a large sample of stars was needed. The less numerous HR-CAT-RRLs catalogue is used instead when an accurate estimation of metallicity and related uncertainties is crucial.

3 METHODS

The methodological approach used in this study is similar to the analysis performed by [Dékány et al. \(2021\)](#), who applied the Se-

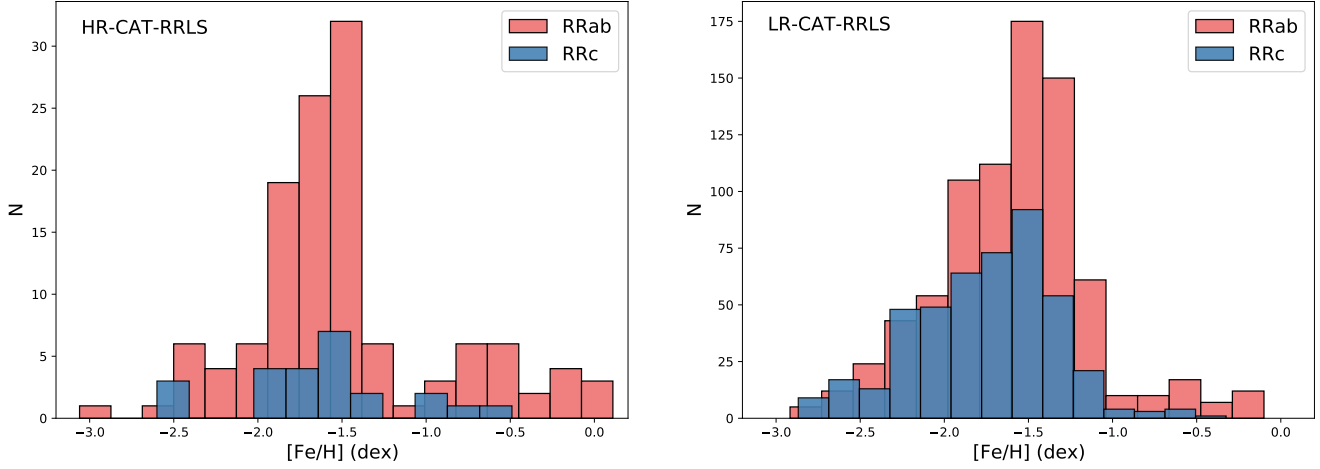


Figure 4. Metallicity distribution of RRLs in the HR-CAT-RRLS (*left panel*) and LR-CAT-RRLS (*right panel*) samples.

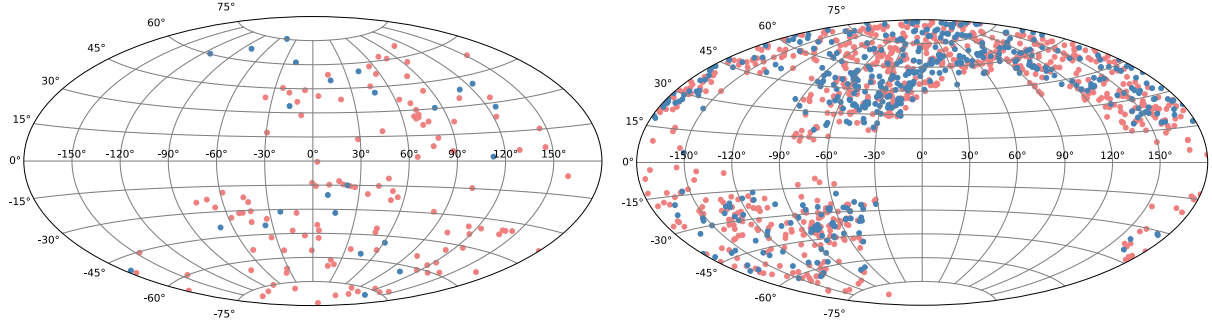


Figure 5. Spatial distribution of RRLs in the HR-CAT-RRLS (*left panel*) and LR-CAT-RRLS (*right panel*) samples.

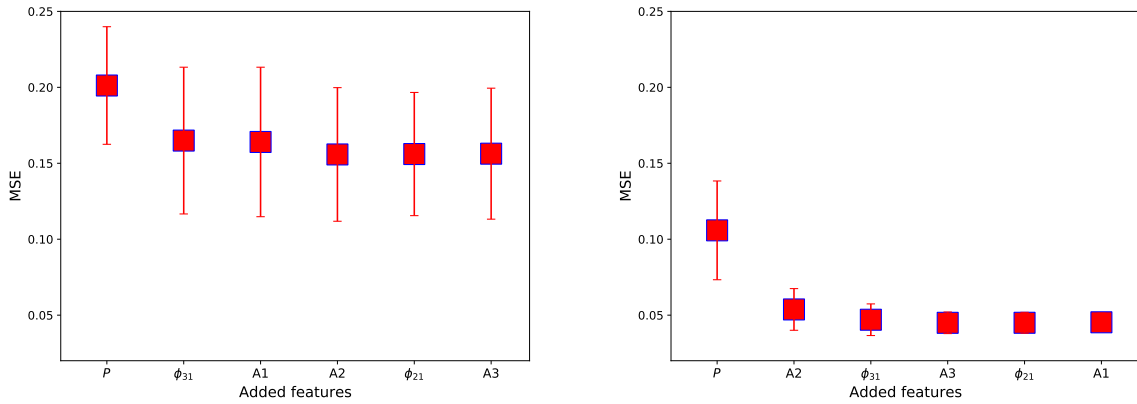


Figure 6. Distribution of the MSE estimated by cross-validation for RRab (*left panel*) and RRc (*right panel*) stars. The X axes show the features subsequently added to the subset.

quential Feature Selection (SFS) and the Bayesian regression to find the photometric metallicities of RRLs from their I -band light curves. In our analysis, we divide the problem of predicting the metallicity of RRLs into two steps: (1) feature selection and (2) application of the Bayesian regression to derive a relation between period, Fourier parameters of the G -band light curves and metallicities.

3.1 Feature selection

Gaia SOS Cep&RRL pipeline (Clementini et al. 2023) represents the G -band light curves of RRLs using a Fourier expansion in cosine functions:

$$\text{mag}(t_j) = z_p + \sum [A_i \cos(i \times 2\pi\nu_{\text{max}}t_j + \phi_i)], \quad (1)$$

where z_p is the zero-point, ν_{max} is the pulsation frequency ($\nu_{\text{max}}=1/P$, where P is the pulsation period), i is the number of harmonics used to model the G -band light curve, A_i are amplitudes and ϕ_i are phases of the Fourier decomposition. The `vari_rrlyrae` table in the *Gaia* DR3 catalogue provides amplitudes and phases of the Fourier decomposition of RRL G -band light curves, as well as phase parameters $\phi_{21} = \phi_2 - 2 * \phi_1$ and $\phi_{31} = \phi_3 - 3 * \phi_1$, and their respective uncertainties (Clementini et al. 2023). While, historically photometric metallicities of RRLs were obtained from the pulsation period and ϕ_{31} parameter (e.g. Jurcsik & Kovacs 1996, Nemeč et al. 2013), in some following studies additional Fourier parameters, such as amplitudes A_1 and A_2 (Dékány et al. 2021) or their ratio $R_{21} = A_2/A_1$ (Li et al. 2023) were used. In our study, we apply the Sequential Feature Selection (SFS) algorithm implemented in the `scikit-learn` software library (Pedregosa et al. 2011) to identify the most relevant features that, in the best way, predict the metallicity of RRab and RRc stars. Since a large sample of RRLs is needed to identify the features correctly, we apply the SFS to the LR-CAT-RRLS sample (Section 2.3). We adopt the forward-SFS algorithm, which is a sequential process starting with an empty set of features and iteratively adding one feature at the time that provides the maximum improvement in model performance. The performance evaluation at each step is done through a cross-validation (CV) algorithm. Namely, after adding each feature, the training sample is divided into five subsets. The model (linear regression in our case) is trained on four subsets, while the fifth is used to evaluate the model performance by computing the mean squared error (MSE). This procedure is repeated for the remaining four subsets, and the final MSE is then the average of the values computed for each subset. Based on this performance evaluation, the algorithm decides which feature should be added to the subset of relevant features. The main advantage of the SFS algorithm is that it explores different feature combinations and evaluates their impact on the model performance. It allows us to identify the most informative features and discard irrelevant or redundant ones, potentially improving the model’s efficiency.

We selected pulsation period P , ϕ_{21} , ϕ_{31} , A_1 , A_2 and A_3 as the initial set of features and run the SFS algorithm to select the most relevant features for predicting the metallicity of 670 RRab stars from the LR-CAT-RRLS, for which all six features were available. The upper section of Table 2 and left panel of Fig. 6 show the distribution of the MSE for different subsets of features. Based on our analysis, the most important features for metallicity prediction of RRab stars are P and ϕ_{31} , while adding A_1 does not improve the MSE performance beyond its uncertainty. Considering that adding more features could cause additional noise, we decide to limit the set of features for RRab stars to $[P, \phi_{31}]$, which is in agreement with previous studies (e.g. Jurcsik & Kovacs 1996, Nemeč et al. 2013).

We repeated the same analysis for 226 RRc stars in the LR-CAT-RRLS, for which all six features were available. Results are shown in the bottom section of Table 2 and the right panel of Fig. 6. The most important features for estimating RRc metallicity are P and A_2 , while adding ϕ_{31} slightly improves the model performance. We, thus, select the set of features $[P, \phi_{31}, A_2]$ for metallicity prediction of RRc stars.

3.2 Bayesian approach

To predict the photometric metallicity of RRLs from the period and Fourier parameters of the G -band light curves, we use the Bayesian

Table 2. Performance of the linear model for different feature sets.

Features	MSE	$\sigma(MSE)$
RRab		
P	0.201	0.039
P, ϕ_{31}	0.165	0.048
P, ϕ_{31} , A_1	0.164	0.049
P, ϕ_{31} , A_1 , A_2	0.156	0.044
P, ϕ_{31} , A_1 , A_2 , ϕ_{21}	0.156	0.041
P, ϕ_{31} , A_1 , A_2 , ϕ_{21} , A_3	0.156	0.043
RRc		
P	0.106	0.032
P, A_2	0.054	0.014
P, A_2 , ϕ_{31}	0.047	0.010
P, A_2 , ϕ_{31} , A_1	0.045	0.007
P, A_2 , ϕ_{31} , A_1 , A_3	0.045	0.007
P, A_2 , ϕ_{31} , A_1 , A_3 , ϕ_{21}	0.045	0.006

fitting approach described in detail by Dékány et al. (2021) and Muraveva et al. (2018b). As discussed in Section 3.1, the most important features to predict RRab metallicities are the period and the ϕ_{31} parameter. As a training set for the Bayesian predictive model, we used 121 RRab stars from the HR-CAT-RRLS, for which both features were available. We used the `pymc3` software library to fit the model. Posterior distributions were calculated applying Hamiltonian Markov chain Monte Carlo (MCMC) simulations using the No-U-Turn Sampler (NUTS, Hoffman & Gelman 2011). Fig. 7 shows the posterior distribution of the parameters of the model and the values of the parameters over the course of the MCMC sampling process. The uncertainties in the period, ϕ_{31} and metallicity, as well as the intrinsic scatter of the relation, were taken into account. Metallicity uncertainties were estimated as described in Section 2.2. Uncertainties in periods provided in the *Gaia* DR3 catalogue (Clementini et al. 2023) are negligibly small ($\sim 10^{-6}$). Nevertheless, in Section 2.2, we found that *Gaia* periods agree with the literature values within 0.001 days. Thus, we adopt this value as the period’s uncertainty. Uncertainty in the Fourier parameter ϕ_{31} was taken from *Gaia* DR3 catalogue (Clementini et al. 2023).

Performing the fitting procedure, we found two strong outliers: SS Gru and WZ Hya. SS Gru is the longest-period star in our sample. In some studies (e.g. Plachy et al. 2021) it is classified as anomalous Cepheid. WZ Hya has the largest values of the ϕ_{31} parameter and corresponding uncertainty $\phi_{31} = 3.41 \pm 0.81$ among all stars in the sample. This value of ϕ_{31} could probably be incorrect, especially considering a relatively small number of transits ($N=27$) used for fitting the light curve. We decide to exclude both stars from our sample as strong outliers.

We found the following relation for the metallicity of RRab stars:

$$[\text{Fe}/\text{H}] = (-5.55 \pm 0.33)P + (0.94 \pm 0.09)\phi_{31} - (0.37 \pm 0.20) \quad (2)$$

The intrinsic dispersion of the fit is $\sigma = 0.21$ dex. The root mean squared error (RMSE) of the predicted metallicities in the training sample is 0.28 dex.

We performed the same analysis for RRc stars. As shown in Section 3.1, the most important features to predict the metallicity of RRc stars are period, A_2 and ϕ_{31} Fourier parameters. The HR-CAT-RRLS sample contains only 14 RRc stars, for which all three parameters are available, which is insufficient to construct a reliable predictive model. Thus, we used RRc stars from the LR-CAT-RRLS sample to fit the relation. However, metallicity values of RRc stars in LR-CAT-RRLS from Liu et al. (2020) are not on the metallicity scale adopted by Crestani et al. (2021), that we used to calibrate the relation of RRab stars from HR-CAT-RRLS (Eq.2). Crestani et al. (2021)

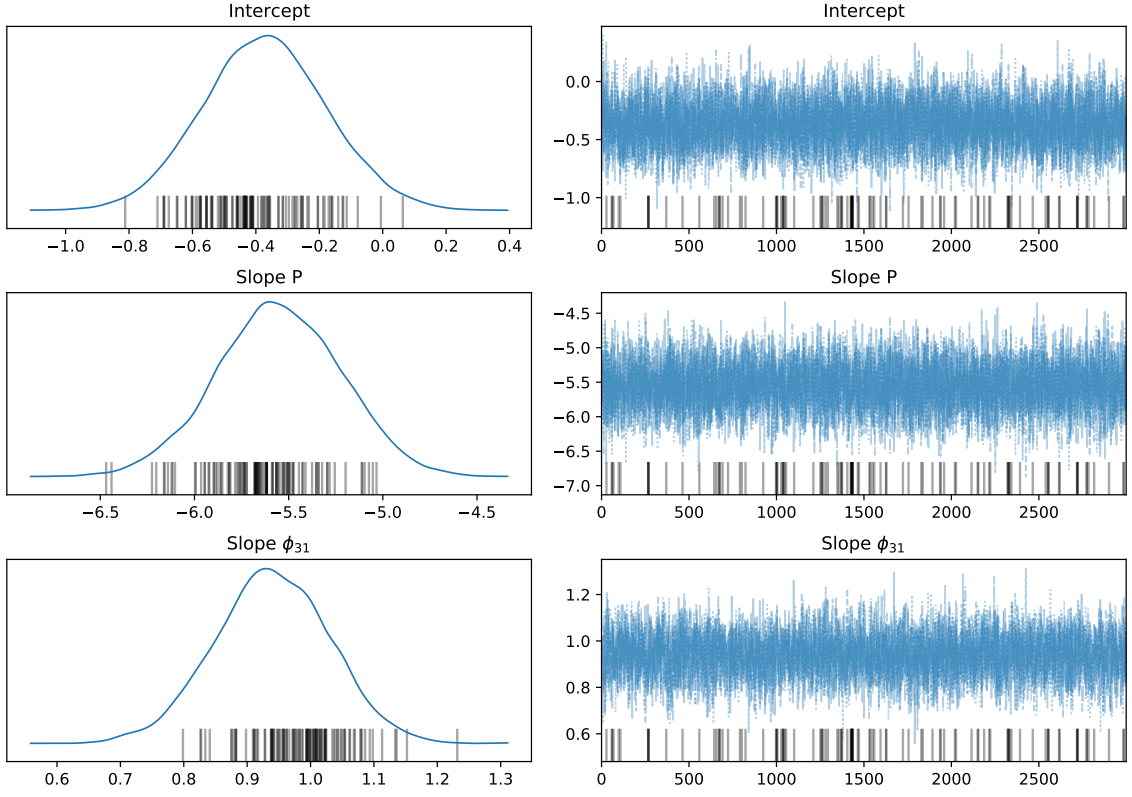


Figure 7. *Left panel:* Posterior distributions of the parameters of the predictive metallicity model for RRAb stars (Eq. 2). *Right panel:* Values of the parameters over the course of the MCMC sampling process. Each point on the X-axis corresponds to a specific sample from the posterior distribution

in their analysis, performed a comparison between their metallicity estimates and values provided by Liu et al. (2020) for 2634 stars in common and found a mean difference of $\Delta = -0.21$ dex for RRc stars. To homogenise the metallicity scales adopted for RRAb stars and RRc stars, we add a shift of +0.21 dex to the metallicity values of RRc stars in the LR-CAT-RRLS sample. In this way, the relations calculated for RRAb and RRc stars in our study are on the same metallicity scale adopted by Crestani et al. (2021).

All three features [P, A_2 , ϕ_{31}] are available for 226 RRc stars from the LR-CAT-RRLS. We applied the Bayesian fitting method and found the following relation for the metallicity of RRc stars:

$$[\text{Fe}/\text{H}] = (-8.54 \pm 0.42)P + (0.23 \pm 0.04)\phi_{31} - (9.34 \pm 1.41)A_2 + (0.80 \pm 0.19) \quad (3)$$

The intrinsic scatter of the fit is $\sigma = 0.19$ dex, while RMSE is 0.21 dex. Fig. 8 shows the posterior distribution of the parameters of the model and the values of the parameters over the course of the MCMC sampling process. In the next section, we perform a validation of our newly derived relations, while in Appendix B we use the XGBoost regressor to explore the potential existence of more complex relationships between light curve parameters and metallicity of RRLs.

4 METALLICITY VALIDATION

We have applied our newly derived relations (Eqs. 2-3) to compute the photometric metallicities of 135,033 RRLs in the GAIA-CAT-

RRLS sample, for which all needed parameters were available. We estimated the uncertainties in metallicity by employing a Monte Carlo simulation approach. For each star, 1000 iterations were performed. The random values were sampled from the error distributions of the period, Fourier parameters and coefficients of the relations (Eqs. 2 - 3), while also simulating the intrinsic dispersion in metallicity (σ). The collection of the metallicity values obtained from the Monte Carlo simulation allowed us to estimate the uncertainties in metallicity.

Applying linear relations to estimate metallicities, we found that for 264 stars (0.002% of the sample), the metallicity reaches unreliable values from -3 up to -5.65 dex at the metal-poor end, and from 1 up to 2.86 dex at the metal-rich end of the metallicity distribution. This is mostly due to unreliable estimates of the period and/or Fourier parameters for a handful of stars. We exclude these stars and remain with a sample of 134,769 RRLs with estimated metallicity values (Table A2). The metallicity distribution of these RRLs is shown in Fig. 9 and spans a total range of $-3.0 < [\text{Fe}/\text{H}] < +1.0$ dex. In particular, there are 178 RRLs with $[\text{Fe}/\text{H}] > +0.1$ dex in the sample, hence they are outside the metallicity range covered by our RRL calibrators ($-3.06 < [\text{Fe}/\text{H}] < +0.11$ dex), Table 1). Their metal abundance should be taken with care. Fig. 10 shows the sky distribution of 134,769 RRLs in our sample, while Fig. 11 shows their Bailey diagram. In both plots the colour encodes the stars' metallicity.

4.1 Comparison with the literature

We have compared the photometric metallicity derived in this study with metallicities estimated from HR spectroscopy, available in the literature (Crestani et al. 2021; Pancino et al. 2015; Gilligan et al.

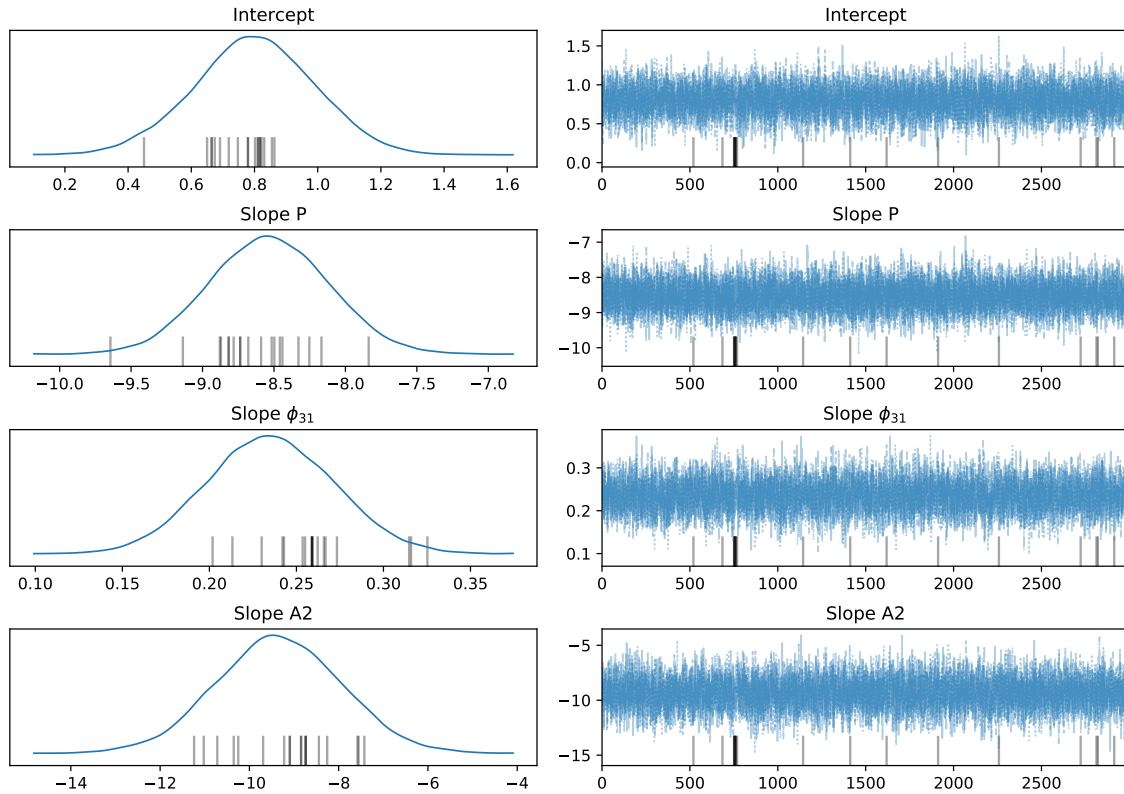


Figure 8. *Left panel:* Posterior distributions of the parameters of the predictive metallicity model for RRC stars (Eq. 3). *Right panel:* Values of the parameters over the course of the MCMC sampling process. Each point on the X-axis corresponds to a specific sample from the posterior distribution

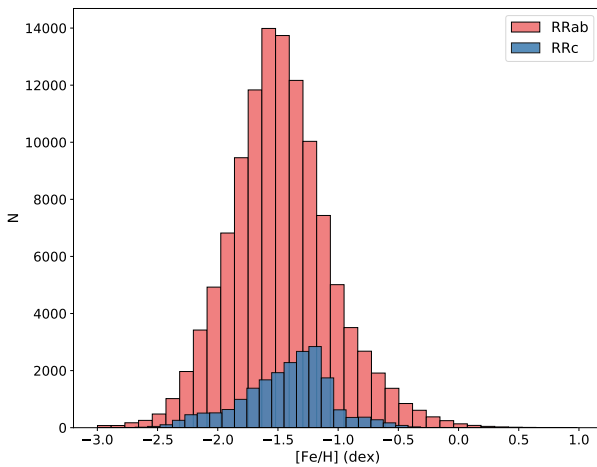


Figure 9. Distribution of metallicities of 134,769 RRLs estimated using Eqs. 2-3

2021; Nemeč et al. 2013). The top panels of Fig. 12 show the comparison between the metallicity estimates, while the bottom panels show the residuals $\Delta[\text{Fe}/\text{H}] = [\text{Fe}/\text{H}]_{\text{spec}} - [\text{Fe}/\text{H}]_{\text{phot}}$. The black dashed line represents the one-to-one relation. The mean residual (Δ) and the rms scatter, calculated with respect to zero residuals, are also shown for each sample. There is a good agreement of our photometric metallicity estimates with the HR-spectroscopic metallicities from Crestani et al. (2021) and Gilligan et al. (2021) with small shifts of $\Delta = -0.04$ dex (rms=0.33 dex) and $\Delta = -0.07$ dex

(rms=0.39 dex), respectively. There are two strong outliers (WZ Hya and V413 Oph) in the first panel of Fig. 12 showing the comparison of our photometric metallicities with values from Crestani et al. (2021) and one strong outlier (WZ Hya) in the third panel, showing the comparison with Gilligan et al. (2021) metallicity estimates. Star V413 Oph (*Gaia* DR3 source_id = 4344296958198114688) was discussed in Section 2.2. Its period from *Gaia* DR3 catalogue differs from the period provided by Crestani et al. (2021), thus, its Fourier parameters and, consequently, photometric metallicity could be incorrect. Star WZ Hya was discussed in Section 3.2, as its Fourier parameters provided in *Gaia* DR3 catalogue could also be incorrect. Excluding both stars from the comparison, we found negligible shifts of $\Delta = -0.02$ dex (rms=0.28 dex) and $\Delta = -0.04$ dex (rms=0.33 dex) between our photometric metallicity estimates and Crestani et al. (2021) and Gilligan et al. (2021) values, respectively. Both samples were used to train our Bayesian predictive model for RRab stars. Agreement between the true and predicted values shows that our model is solid.

At the same time, there are non-negligible shifts between our photometric metallicities and the metallicity values from Pancino et al. (2015) and Nemeč et al. (2013): $\Delta = 0.13$ dex (rms = 0.26 dex) and $\Delta = 0.25$ dex (rms=0.39 dex), respectively, with our values being more metal-poor. The same trend was found by Crestani et al. (2021), when they made a comparison between their HR-spectroscopic metallicities and those of Nemeč et al. (2013) and Pancino et al. (2015) (see Table 4 in Crestani et al. 2021). Thus, the shift that we see in Fig 12 is mainly related to the shifts between the metallicity scales adopted by Crestani et al. (2021) and those adopted by Pancino et al. (2015) and Nemeč et al. (2013).

We also compared our photometric metallicities with the metallic-

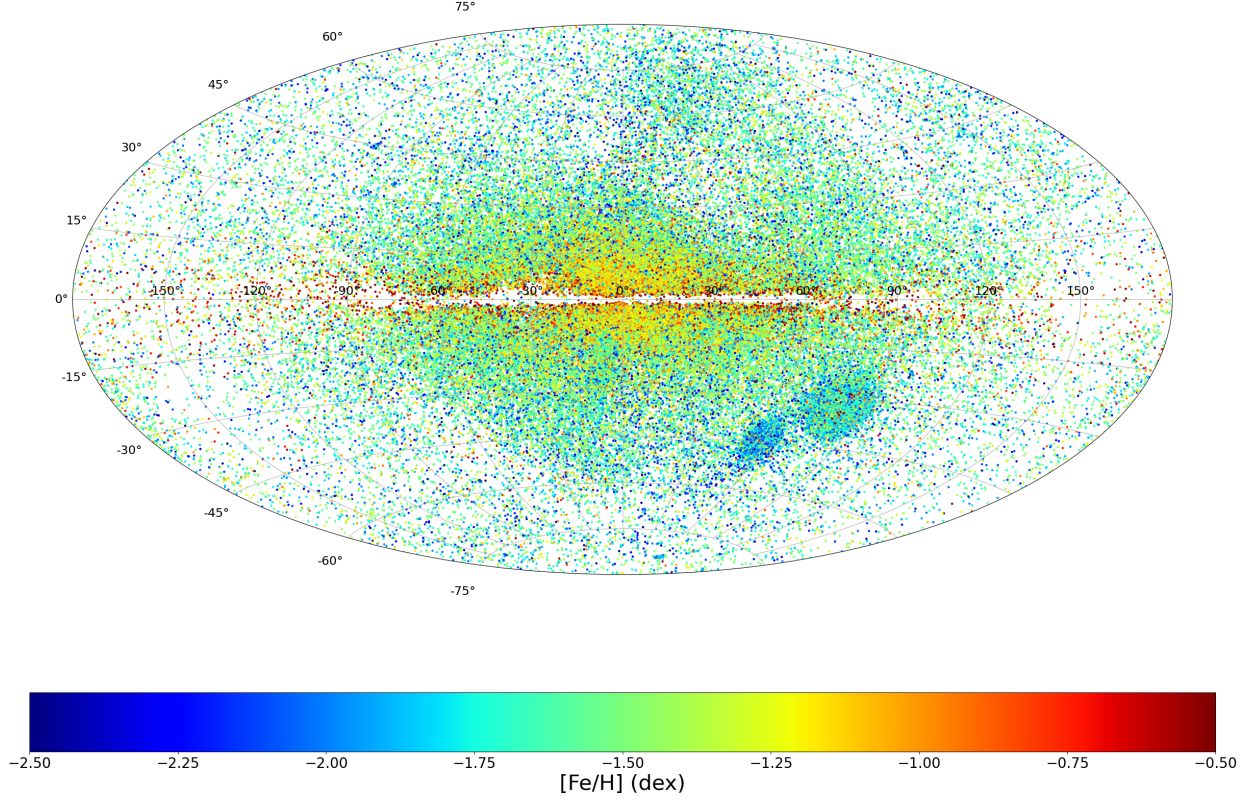


Figure 10. Sky distribution of 134,769 RRLs from the GAIA-CAT-RRLS sample. Sources are colour-coded according to the metal abundance obtained using Eqs. 2 and 3. There are 803 RRLs with $-3.0 < [\text{Fe}/\text{H}] < -2.5$ dex (all shown in dark blue) and 2557 RRLs with $[\text{Fe}/\text{H}] > -0.5$ dex (shown in dark red).

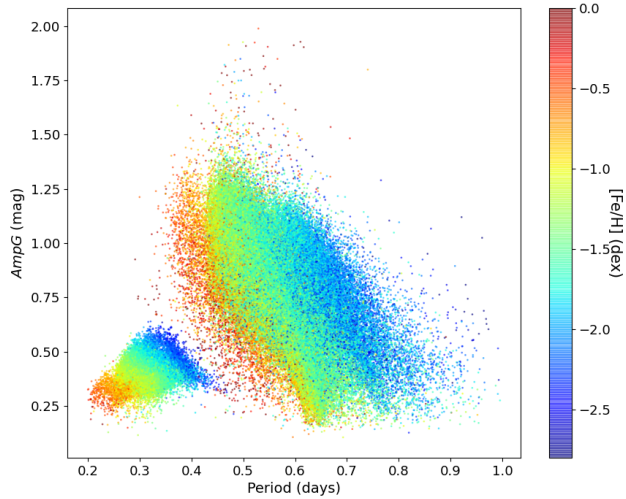


Figure 11. Amplitude in the G -band versus period distribution of the 134,769 RRLs from the GAIA-CAT-RRLS sample, colour-coded according to the photometric metallicity obtained using Eqs. 2 and 3.

ities from LR-spectroscopy (Zinn et al. 2020; Liu et al. 2020). This comparison is shown in Fig. 13. We found an excellent agreement between our values and those of Zinn et al. (2020) with a shift of $\Delta = 0$ dex and rms of 0.31 dex. The shift between LR-spectroscopic metallicity values from Liu et al. (2020) and our estimates is mild $\Delta = -0.05$ dex (rms=0.35 dex). Still, the right panel of Fig. 13

clearly shows that our photometric metallicities are systematically higher than Liu et al. (2020)’s, particularly for RRc stars. This finding is in agreement with the shift of 0.21 dex between Crestani et al. (2021) and Liu et al. (2020) metallicity values found by Crestani et al. (2021) and discussed in Section 3.2.

Finally, we compared our $[\text{Fe}/\text{H}]$ estimates and the photometric metallicities of RRLs calculated using the *Gaia* G -band photometry by Iorio & Belokurov (2021), Dékány & Grebel (2022), Li et al. (2023) and Clementini et al. (2023). Iorio & Belokurov (2021) calibrated the $P - \phi_{31} - [\text{Fe}/\text{H}]$ relation using a sample of 84 RRab stars from Layden (1994) with metallicities from low-to-moderate-resolution spectroscopy and period and ϕ_{31} Fourier parameter from the *Gaia* DR2 catalogue (Clementini et al. 2019). They calibrated the relation for RRc stars using members of GCs assuming as metallicities the spectroscopic values of the corresponding clusters in the Harris (2010) catalogue. Metal abundances of Iorio & Belokurov (2021) are on the Zinn & West (1984) metallicity scale. To make a comparison with our metallicity estimates which are on the metallicity scale adopted by Crestani et al. (2021), we firstly transformed the metallicity values from Iorio & Belokurov (2021) to the Carretta et al. (2009) scale using the relation: $[\text{Fe}/\text{H}]_{\text{C09}} = 1.105[\text{Fe}/\text{H}]_{\text{ZW84}} + 0.160$ (Carretta et al. 2009). We then converted them to the scale adopted by Crestani et al. (2021), adding a shift of 0.08 dex according to Crestani et al. (2021) and Mullen et al. (2021). The first two panels of Fig. 14 show the comparison between our metallicity estimates and the metal abundances from Iorio & Belokurov (2021) for RRab (upper panel) and RRc stars (bottom panel), respectively. There is an excellent agreement between the two metallicity estimates with a mild shift of $\Delta = 0.04$ dex (rms=0.13 dex) for RRc stars, while

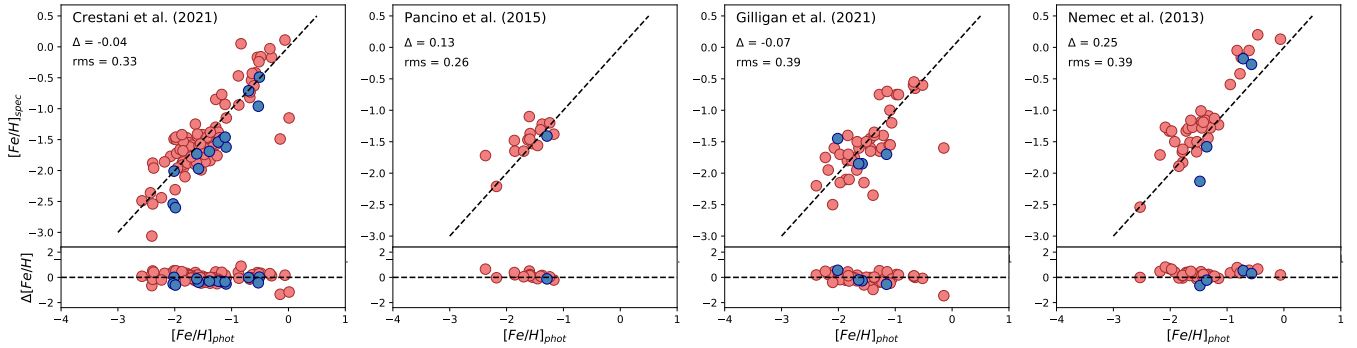


Figure 12. Comparison between photometric metallicity values calculated using Eqs. 2-3 and HR-spectroscopic metallicities from the literature for RRab (red circles) and RRc (blue circles) stars. Black dashed lines in the upper panels represent the one-to-one relations. The bottom panels show residuals $\Delta[Fe/H] = [Fe/H]_{spec} - [Fe/H]_{phot}$.

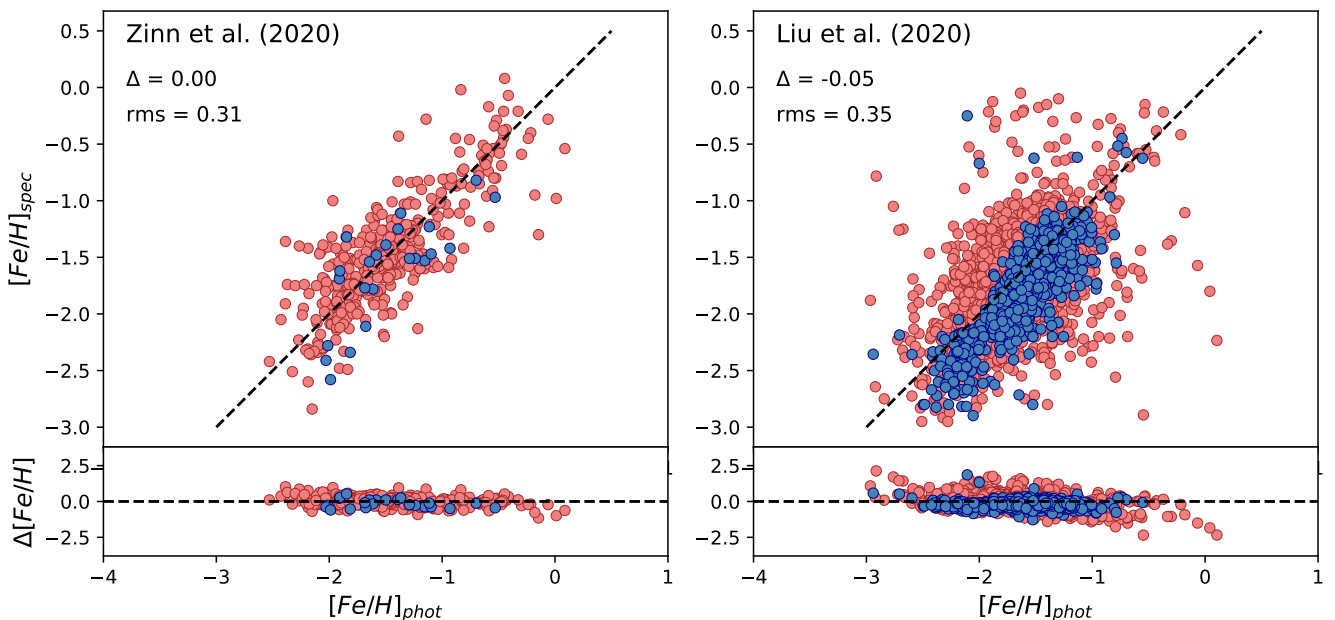


Figure 13. Comparison between photometric metallicity values calculated using Eqs. 2-3 and LR-spectroscopic metallicities from different studies in the literature for RRab (red circles) and RRc (blue circles) stars. Black dashed lines in the upper panels represent the one-to-one relations. The bottom panels show the residuals $\Delta[Fe/H] = [Fe/H]_{spec} - [Fe/H]_{phot}$.

there is a clear offset of $\Delta = 0.16$ dex (rms=0.19 dex) for RRab stars. Values of metallicity from [Iorio & Belokurov \(2021\)](#) are more metal-rich for low metallicities and more metal-poor for high metallicities. This offset could be due to differences in the training sets used to calibrate the relations (RRLs from [Crestani et al. 2021](#) in our study versus [Layden 1994](#) RRL sample in [Iorio & Belokurov 2021](#)), and differences in period and Fourier parameters of the RRLs (*Gaia* DR2 in [Iorio & Belokurov 2021](#) versus *Gaia* DR3 in this study).

[Dékány & Grebel \(2022\)](#) used deep learning algorithms to calculate metallicities of $\sim 60,000$ RRab stars from the *G*-band light curves published in *Gaia* DR2. The metallicity of the training sample of RRLs was estimated using empirical relations derived for the *I*-band photometry, which were calibrated based on the sample of RRLs with HR-spectroscopic estimates of metallicity ([Dékány et al. 2021](#)). The training set used by [Dékány et al. \(2021\)](#) consists of RRLs with HR-spectroscopic measurements from [Crestani et al. \(2021\)](#), [Clementini et al. \(1995\)](#), [Fernley & Barnes \(1996\)](#), [Lambert et al. \(1996\)](#), [Liu et al. \(2013\)](#), [Nemec et al. \(2013\)](#), [Govea et al. \(2014\)](#),

[Pancino et al. \(2015\)](#) and [Andrievsky et al. \(2018\)](#). The second panel of Fig. 14 shows the comparison of our photometric $[Fe/H]$ estimates and values from [Dékány et al. \(2021\)](#) for RRab stars. Even though there is a reasonable agreement between the two datasets, there is still an offset of $\Delta = -0.19$ dex with 0.31 dex scatter. This could be due to the different methods applied to predict metallicity (Bayesian regression versus deep learning algorithms) and differences in the training sets.

Recently, [Li et al. \(2023\)](#) published $P - \phi_{31} - R_{21} - [Fe/H]$ and $P - R_{21} - [Fe/H]$ relations for RRab and RRc stars, respectively, calibrated using period and Fourier parameters from the *Gaia* DR3 catalogue and metallicities from LR-spectroscopy ([Liu et al. 2020](#)). The third panels of Fig. 14 show a comparison of our results with estimates from [Li et al. \(2023\)](#). For RRab stars, we found a negligible shift of $\Delta = -0.01$ dex (rms=0.11 dex) between our estimates and [Li et al. \(2023\)](#), with the latter being metallicities being higher at the metal-rich end and lower than ours at the metal-poor end. [Li et al. \(2023\)](#) metallicities for RRc stars are instead lower than ours ($\Delta =$

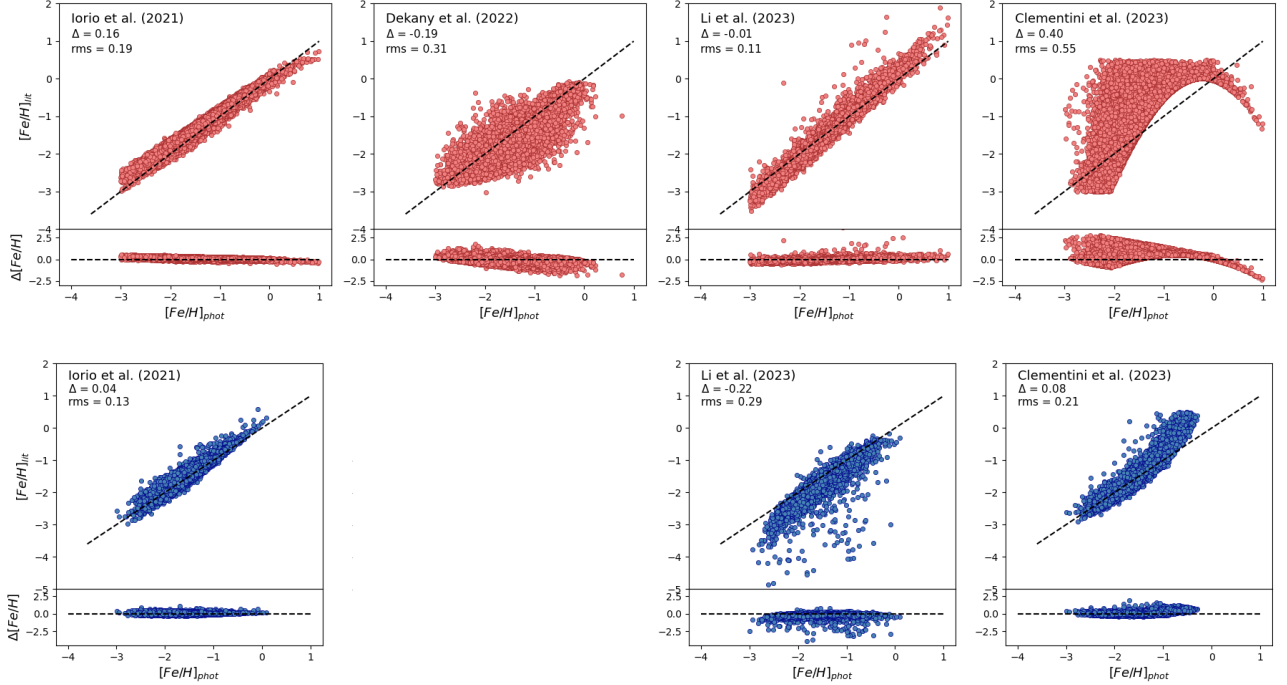


Figure 14. Comparison between photometric metallicity values calculated using Eqs. 2-3 and metallicities from different studies in the literature calculated using *Gaia* data for RRAb (red circles) and RRc (blue circles) stars. Black dashed lines in the upper panels represent the one-to-one relations. The bottom panels in each plot show the residuals $\Delta[\text{Fe}/\text{H}] = [\text{Fe}/\text{H}]_{\text{lit}} - [\text{Fe}/\text{H}]_{\text{phot}}$.

-0.22 dex, rms=0.29 dex) over the whole metallicity range. This shift could be due to the offset of 0.21 dex (Crestani et al. 2021) between the training sample used to calibrate metallicities in our analysis and the training sample of stars with the LR-spectroscopic measurements from Liu et al. (2020) used by Li et al. (2023) to calibrate their relation (see Section 3.2). It is also worth noting that Li et al. (2023) estimated the metallicities of RRAb stars from $P - \phi_{31} - R_{21} - [\text{Fe}/\text{H}]$ relation, where $R_{21} = A_2/A_1$, while we used $P - \phi_{31} - [\text{Fe}/\text{H}]$ relation. At the same time metallicities of RRc stars were estimated by Li et al. (2023) using a $P - R_{21} - [\text{Fe}/\text{H}]$ relation, while a $P - \phi_{31} - A_2 - [\text{Fe}/\text{H}]$ relation was applied in our study. This may also have contributed to the larger discrepancy with our estimates, especially, for RRc stars.

Finally, we compared our metallicities with the values provided in the *Gaia* DR3 catalogue (Clementini et al. 2023). Results are shown in the fourth panels of Fig. 14. The metallicity values of RRLs in *Gaia* catalogue (both for DR2 and DR3) are derived from quadratic relations published by Nemeč et al. (2013). Those relations are calibrated using 41 RRLs (37 RRAb and 4 RRc stars) with metal abundances from HR spectra observed in the field-of-view of the *Kepler* space telescope. A sequence of transformations between the *Gaia* *G*-band and the *Kepler* photometric system were necessary to apply Nemeč et al. (2013) relations (see details in Sect. 2.1.1 of Clementini et al. 2019), which could potentially have caused additional systematic errors. This may explain the discrepancy between metallicity estimates in this study and RRL metallicities in the *Gaia* DR3 catalogue seen in Fig. 14.

4.2 Metallicity in GCs

To further test the quality of our metallicity estimates, we analysed RRLs from our sample belonging to MW GCs whose metal abundance from HR spectra is available in the literature. We used a

compilation from the literature to select the member stars of GCs. As a reference compilation of RRLs identified as members of the MW GCs, we have adopted the Clement et al. (2001)’s catalogue¹. This catalogue which is constantly updated from the literature, summarizes numbers and types of variable stars in GCs. We restricted our analysis only to GCs with more than five RRLs, for which we estimated a photometric metallicity using Eqs. 2-3. As a result, we selected 785 RRLs belonging to 38 GCs (Table 3). Fig. 15 shows metallicity versus period for RRAb (red dots) and RRc (blue dots) stars in GCs with 10 or more RRLs. We transformed our photometric metallicities that are estimated on the metallicity scale adopted by Crestani et al. (2021) to Carretta et al. (2009) metallicity scale by subtracting 0.08 dex from our values (Crestani et al. 2021; Mullen et al. 2021). Black dashed lines represent the Carretta et al. (2009)’s metallicity for the GCs. Differences between Carretta et al. (2009) values and the mean metallicity we infer from the GC RRLs are labelled (Δ), along with the standard deviation (std) of individual RRL metallicities from the mean values. Carretta et al. (2009) did not provide metallicity estimate for the GC NGC 6426, thus, we use metallicity value from Harris (2010) for this cluster.

Even though GCs can host different stellar population, metallicity of RRLs in the same GC are expected to have similar values. Fig. 15 allows us to check (1) if the scatter in metallicity of RRLs in the same cluster (std) is reasonably small; (2) if there is any dependence of our metallicity values on period, which can hint to some bias in our method; (3) if there is consistency between $[\text{Fe}/\text{H}]$ values of RRAb and RRc stars in the same cluster; (4) if there is consistency between our mean photometric metallicities for RRLs and the GC metallicities from Carretta et al. (2009). We see that apart from some clusters (e.g.

¹ <https://www.astro.utoronto.ca/~cclement/cat/listngc.html>

Table 3. Parameters for 38 GCs containing more than 5 RRLs, for which we estimated photometric metallicity using Eqs. 2-3: (1) name of the GC; (2) and (3) mean value and standard deviation of the metallicity estimates of the RRLs in each GC on [Crestani et al. \(2021\)](#) metallicity scale calculated using Eqs. 2-3; (4) and (5) metallicity and corresponding uncertainty of GCs from [Carretta et al. \(2009\)](#); (6) and (7) mean value and standard deviation of the GC's distance moduli, calculated using individual distance estimates to the RRLs in each GC; (8) reddening value from [Harris \(2010\)](#); (9) number of RRLs in the GC with photometric metallicity estimates.

Name	[Fe/H] _{RRLS} (dex)	σ [Fe/H] _{RRLS} (dex)	[Fe/H] _{C09} (dex)	σ [Fe/H] _{C09} (dex)	μ (mag)	$\sigma\mu$ (mag)	E(B-V) (mag)	N_{RRLS}
NGC 362	-1.52	0.22	-1.30	0.04	14.67	0.06	0.05	14
NGC 1261	-1.54	0.21	-1.27	0.08	16.02	0.10	0.01	13
NGC 1851	-1.57	0.30	-1.18	0.08	15.42	0.08	0.02	21
NGC 2419	-1.97	0.22	-2.20	0.09	19.56	0.06	0.08	9
NGC 3201	-1.63	0.15	-1.51	0.02	13.42	0.09	0.24	70
NGC 4147	-1.61	0.04	-1.78	0.08	16.33	0.06	0.02	6
Rup 106	-1.80	0.13	-1.78	0.08	16.73	0.35	0.20	13
NGC 4590 (M68)	-2.16	0.15	-2.27	0.04	15.06	0.07	0.05	20
NGC 4833	-2.08	0.11	-1.89	0.05	13.98	0.09	0.32	9
NGC 5024 (M53)	-2.06	0.20	-2.06	0.09	16.27	0.06	0.02	26
NGC 5053	-2.05	0.18	-2.30	0.08	16.14	0.07	0.01	8
NGC 5139	-1.73	0.40	-1.64	0.09	13.63	0.37	0.12	36
NGC 5272 (M3)	-1.71	0.24	-1.50	0.05	15.03	0.09	0.01	23
NGC 5466	-1.94	0.26	-2.31	0.09	15.98	0.04	0	13
IC 4499	-1.74	0.22	-1.62	0.09	16.44	0.07	0.23	61
NGC 5824	-2.00	0.23	-1.94	0.14	17.52	0.08	0.13	16
NGC 5904 (M5)	-1.57	0.28	-1.33	0.02	14.33	0.09	0.03	38
NGC 5986	-1.86	0.19	-1.63	0.08	15.09	0.05	0.28	6
NGC 6093 (M80)	-2.05	0.31	-1.75	0.08	15.00	0.33	0.18	6
NGC 6121 (M4)	-1.31	0.16	-1.18	0.02	11.60	0.13	0.35	39
NGC 6171 (M107)	-1.20	0.14	-1.03	0.02	14.01	0.40	0.33	22
NGC 6229	-1.51	0.25	-1.43	0.09	17.38	0.07	0.01	26
NGC 6304	-1.58	0.50	-0.37	0.07	14.63	0.25	0.54	6
NGC 6341 (M92)	-2.13	0.11	-2.35	0.05	14.57	0.03	0.02	8
NGC 6333 (M9)	-1.74	0.31	-1.79	0.09	15.00	0.61	0.38	9
NGC 6362	-1.29	0.20	-1.07	0.05	14.36	0.06	0.09	25
NGC 6426	-2.10	0.29	-	-	16.13	0.82	0.36	10
NGC 6584	-1.63	0.22	-1.50	0.09	15.64	0.07	0.10	30
NGC 6638	-1.37	0.20	-0.99	0.07	14.77	0.23	0.41	6
NGC 6642	-1.33	0.24	-1.19	0.14	14.49	0.13	0.40	6
NGC 6712	-1.33	0.09	-1.02	0.07	14.19	0.05	0.45	6
NGC 6723	-1.34	0.28	-1.10	0.07	14.59	0.07	0.05	9
NGC 6864 (M75)	-1.52	0.32	-1.29	0.14	16.55	0.11	0.16	7
NGC 6934	-1.68	0.20	-1.56	0.09	15.99	0.06	0.10	47
NGC 6981 (M72)	-1.71	0.26	-1.48	0.07	16.15	0.12	0.05	33
NGC 7006	-1.69	0.28	-1.46	0.06	18.11	0.07	0.05	30
NGC 7078 (M15)	-2.19	0.26	-2.33	0.02	15.08	0.08	0.10	44
NGC 7089 (M2)	-1.94	0.23	-1.66	0.07	15.23	0.04	0.06	14

NGC 5139, NGC 1851), the scatter of RRLs belonging to the same cluster is relatively small (less than 0.3 dex) and consistent with uncertainties in individual measurements (~ 0.4 dex). We do not see any significant dependence of the metallicity on period. Metallicities of RRab and RRc stars in the same cluster are in good agreement. Apart from a few GCs (e.g. NGC 1851, NGC 5466), our metallicity estimates also agree with [Carretta et al. \(2009\)](#) values. In addition, we found that our method can predict metallicities of both metal-poor (e.g. NGC 7078, NGC 5024, NGC 6426, NGC 4590) and metal-rich clusters (e.g. NGC 6121, NGC 6171) with good accuracy.

Fig. 16 shows the comparison between metallicities of GCs from [Carretta et al. \(2009\)](#) and weighted mean of our photometric [Fe/H] estimates of RRLs for each cluster. Only clusters with 10 or more RRLs are shown. Errors in the mean metallicity of RRLs are calculated as the standard deviation of the mean value. As shown in Fig. 16 our values are consistent with the metallicities from [Carretta et al. \(2009\)](#) within the errors.

5 DISTANCES TO RR LYRAE STARS

We used the metallicity values derived in the previous sections to calculate individual distances to the RRLs in our sample. Following the approach of [Li et al. \(2023\)](#), we adopted $E(B - V)$ reddening values from [Schlegel et al. \(1998\)](#) for the majority of stars. For RRLs located in the Magellanic Clouds, we adopted instead values of $E(V - I)$ from [Skowron et al. \(2021\)](#), which we transformed to $E(B - V)$ using the relation $E(B - V) = E(V - I)/1.318$ from [Skowron et al. \(2021\)](#). Finally, we used reddening values from [Harris \(2010\)](#) for RRLs in GCs. In this way, we were able to find reddening values for 134,665 stars, for which we have photometric metallicities estimated with Eqs. 2-3. Uncertainties of the reddening values were taken from the corresponding studies apart from [Harris \(2010\)](#) values, for which we adopted a reddening uncertainty of 0.05 mag. Individual extinction values were calculated using the total-to-selective extinction ratio $R_G = 2.516 \pm 0.036$ ([Huang et al. 2021](#)).

Distances were calculated using the $M_G - [\text{Fe}/\text{H}]$ relation by [Garofalo et al. 2022](#) (their Eq. 18), which was calibrated using the

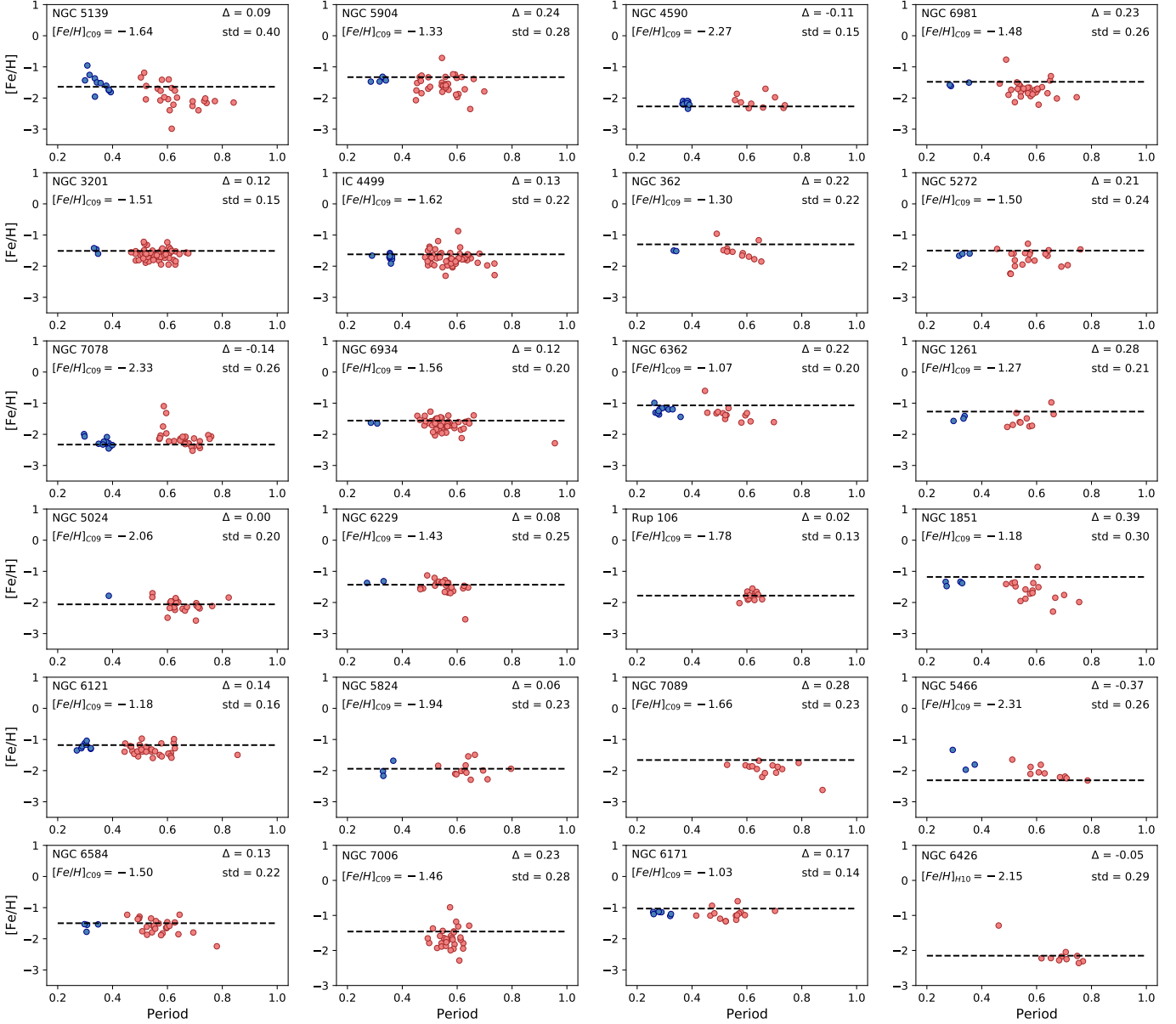


Figure 15. Photometric metallicities of RRLs calculated in this study plotted versus period for RRab (red dots) and RRc (blue dots) stars in 24 GCs of those listed in Table 3, that contain 10 or more RRLs. Black dashed lines show the GC metallicity from Carretta et al. (2009). The shift between the metallicity of GC from Carretta et al. (2009) and the mean metallicity of RRLs in the GC is labelled (Δ) along with the standard deviation (std) of individual RRL metallicity estimates around the mean value. Carretta et al. (2009) did not provide a metallicity estimate for NGC 6426, thus, we use the metallicity value from Harris (2010) for this cluster.

hierarchical Bayesian approach and accurate parallaxes of bright MW RRLs published in the *Gaia* EDR3 catalogue. Garofalo et al. (2022) used metallicities of GCs on the Carretta et al. (2009) metallicity scale. Thus, we transformed our metallicity values to the Carretta et al. (2009) scale by subtracting 0.08 dex. For a handful of stars (23, 0.0002% of the sample) in the central region of the disk, the obtained distance moduli have non-physical negative values due to significantly overestimated reddening. We discarded these stars, thus

remaining with a sample of 134,642 RRLs with individual distance estimates.

Uncertainties in our distance estimates come from uncertainties in extinction and individual metallicity values (see Section 4), uncertainties in the coefficients of the $M_G - [\text{Fe}/\text{H}]$ relation, and intrinsic scatter of the fit ($\sigma = 0.13$). We estimated the uncertainties in distance moduli using a Monte Carlo simulation approach. For each star, 1000 iterations were performed. The random values were sampled from the

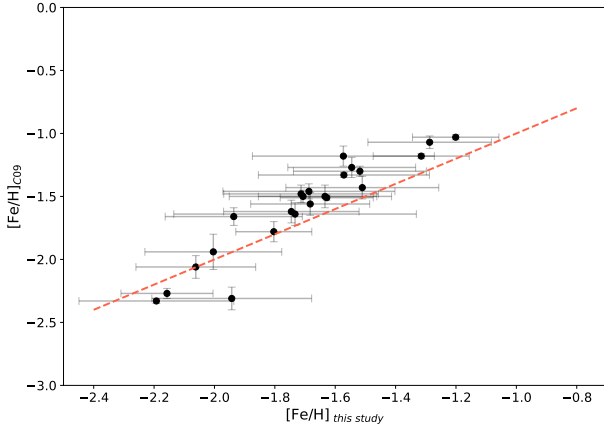


Figure 16. Comparison between the metallicity of GCs from Carretta et al. (2009) and the mean photometric metallicity of RRLs in the GCs calculated in this study. Only GCs containing 10 or more RRLs with photometric metallicity estimates are shown. The red dashed line represents the one-to-one relation.

error distributions of extinction, metallicity and coefficients, while also simulating the intrinsic dispersion of the $M_G - [\text{Fe}/\text{H}]$ relation (σ). Collecting the distance values obtained from the Monte Carlo simulation allowed us to estimate uncertainties in distance moduli.

The sky distribution of the 134,642 RRLs in our sample, colour-coded by distance, is shown in Fig. 17. The closest stars to us are located in the disk of the MW, as expected. The Sagittarius (Sgr) stream and core are clearly seen. In Table 3 we report mean value and standard deviation of the GC’s distance moduli, calculated using individual distance estimates to the RRLs in each GC.

Finally, we calculated the 3-D positions of the RRLs in our sample from their coordinates and estimated distances. The position of the Sun was assumed to be on the X-axis of the right-handed system. The X-axis points from the position of the Sun to the Galactic centre, while the Y-axis points towards Galactic longitude $l = 90^\circ$. The Z-axis points towards the North Galactic Pole ($b = 90^\circ$). The Sun was assumed to be at a distance of 8.122 kpc from the Galactic centre (GRAVITY Collaboration et al. 2018). Fig. 18 shows the distribution of RRLs on the X-Z (left panel) and Y-Z (right panel) planes. Well-known structures, such as the Large Magellanic Cloud (LMC), Small Magellanic Cloud (SMC), the Sgr stream and the core of the Sgr dwarf spheroidal galaxy are clearly seen. This shows the potential of distance and metallicity measurements of RRLs obtained in this work for studying substructures, located in and outside of our Galaxy.

6 THE MAGELLANIC CLOUDS

To evaluate the quality of our distance and metallicity estimates, we analyse RRLs located in the LMC and SMC, the biggest MW satellites traditionally used as laboratories for studying different stellar populations. Cusano et al. (2021) analysed a sample of $\sim 22,000$ RRLs located in the LMC, whose membership was confirmed by means of the PL relation in the K_s band. We cross-matched this catalogue against our sample of RRLs with photometric metallicity and distance estimates and found 12,239 stars in common. The metallicity distribution of these LMC RRLs is shown by the orange histogram in Fig. 19. The weighted mean photometric metallicity of the RRLs in the LMC is $[\text{Fe}/\text{H}]_{\text{LMC}} = -1.63 \pm 0.36$ dex, where the uncertainty is calculated as the standard deviation of

the mean value. This metallicity value is in good agreement with $[\text{Fe}/\text{H}]_{\text{LMC}} = -1.48 \pm 0.03 \pm 0.06$ dex measured by Gratton et al. (2004) from low-resolution spectra of 98 RRLs in the bar of the LMC and $[\text{Fe}/\text{H}]_{\text{LMC}} = -1.53 \pm 0.02$ dex reported by Borissova et al. (2006) based on the analysis of 100 RRLs in the LMC. Skowron et al. (2016) obtained the median value of photometric metallicities of RRLs in the LMC $[\text{Fe}/\text{H}]_{\text{ZW84}} = -1.59 \pm 0.31$ on the Zinn & West (1984) metallicity scale that once transformed to the metallicity scale adopted by Crestani et al. (2021) used in the present study (see Sect. 4.1) provides the value $[\text{Fe}/\text{H}]_{\text{C21}} = -1.52$ dex in good agreement with our estimate. We also measured a mean distance modulus for the RRLs in the LMC: $\mu_{\text{LMC}} = 18.55 \pm 0.18$ mag, in good agreement within the errors with previous measurements based on Cepheids ($\mu_{\text{LMC}} = 18.477 \pm 0.033$ mag, Freedman et al. 2012), RRLs ($\mu_{\text{LMC}} = 18.50 \pm 0.16$ mag, Muraveva et al. 2018c) and eclipsing binaries ($\mu_{\text{LMC}} = 18.48 \pm 0.03$ mag, Pietrzyński et al. 2019).

In Muraveva et al. (2018a), we analysed 2997 fundamental mode RRLs, which were confirmed to belong to the SMC based on their position on the PL relation in the K_s band. We cross-matched this catalogue against our sample of RRLs with photometric metallicity and distance estimates and found 2203 stars in common. Their metallicity distribution is shown by the green histogram in Fig. 19. The weighted mean metallicity of the RRLs in the SMC is $[\text{Fe}/\text{H}]_{\text{SMC}} = -1.86 \pm 0.36$ dex in perfect agreement with the value $[\text{Fe}/\text{H}]_{\text{C21}} = -1.80$ dex, obtained by transforming to Crestani et al. (2021) metallicity scale the value $[\text{Fe}/\text{H}]_{\text{SMC}} = -1.85 \pm 0.35$ dex on the Zinn & West (1984) scale derived by Skowron et al. (2016). The mean distance modulus of the SMC from RRLs is $\mu_{\text{SMC}} = 19.01 \pm 0.17$ mag in good agreement within the errors with previous values based on Cepheids ($\mu_{\text{SMC}} = 18.96 \pm 0.01 \pm 0.03$ mag, Scowcroft et al. 2016) and eclipsing binaries ($\mu_{\text{SMC}} = 18.977 \pm 0.016 \pm 0.028$ mag, Graczyk et al. 2020).

Fig. 20 shows the sky distribution of the RRLs in the LMC and SMC with the colour encoding the individual distance moduli of the stars. It is clearly seen that, as expected, the SMC is located farther from us than the LMC. Moreover, the north-eastern part of the LMC, as traced by RRLs, is closer to us than the south-western part, which has already been reported in the literature (e.g. Cusano et al. 2021). This once again confirms the reliability of our distance estimates.

7 SUMMARY

We have obtained new $P - \phi_{31} - [\text{Fe}/\text{H}]$ and $P - \phi_{31} - A_2 - [\text{Fe}/\text{H}]$ relations for RRab and RRc stars, respectively. The relations are based on the periods and Fourier parameters of the *Gaia* G -band light curves of RRLs published in *Gaia* DR3 and spectroscopic metallicities of RRLs available in the literature. Both relations are calibrated on the metallicity scale adopted by Crestani et al. (2021). We applied a feature selection procedure based on the cross-validation to choose the parameters most relevant for metallicity determination. The relations were derived using the Bayesian fitting approach which allowed us to carefully take into account uncertainties in the parameters and the intrinsic scatter of the fit. The RMSE of the predicted metallicity values for the RRLs in the training sample are 0.28 dex and 0.21 dex for RRab and RRc stars, respectively, comparable with the typical uncertainty of metallicity measurements from LR spectroscopy.

We applied the newly derived relations to estimate the metallicity of 134,769 RRLs from the *Gaia* DR3 catalogue. We compared our metallicities with metallicity estimates from HR- and LR-spectroscopy and with photometric metallicities available in the lit-

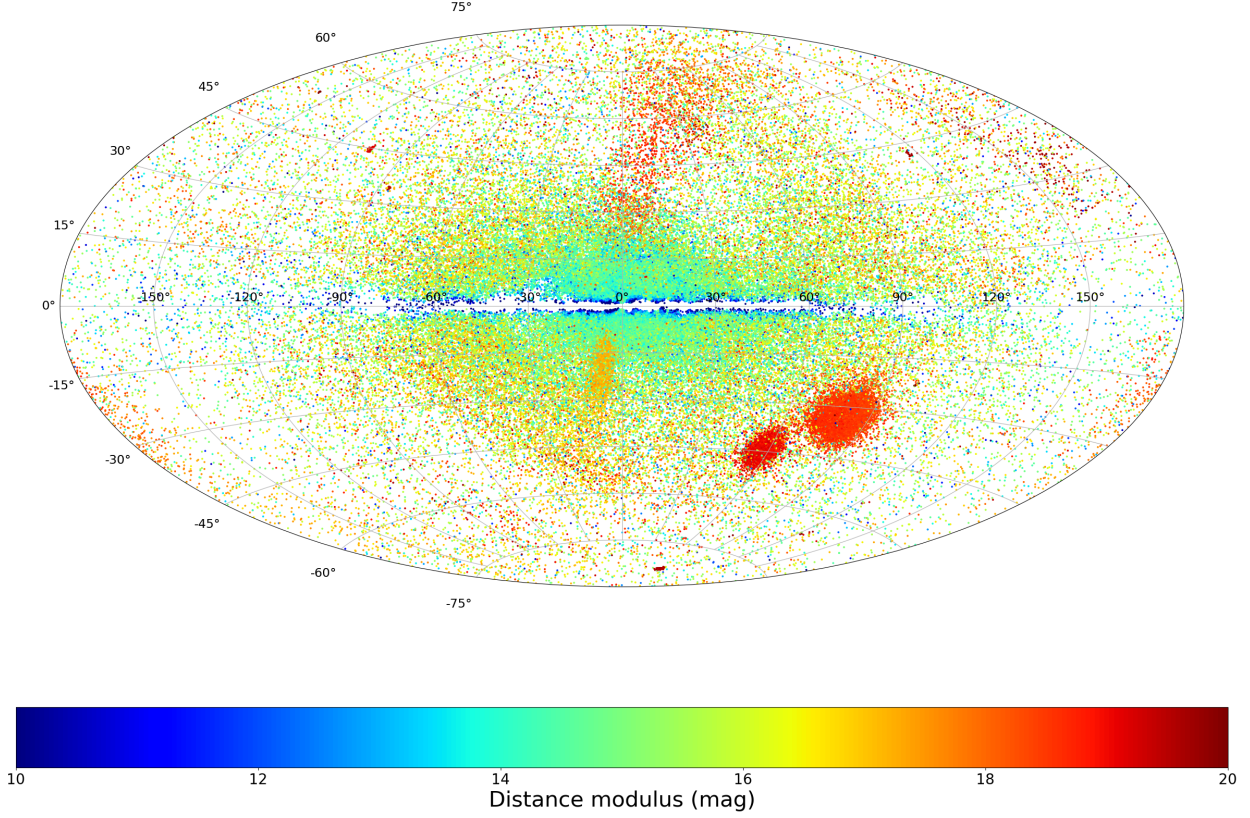


Figure 17. Sky distribution of the 134,642 RRLs with individual distances estimated in this study. Sources are colour-coded by distance modulus.

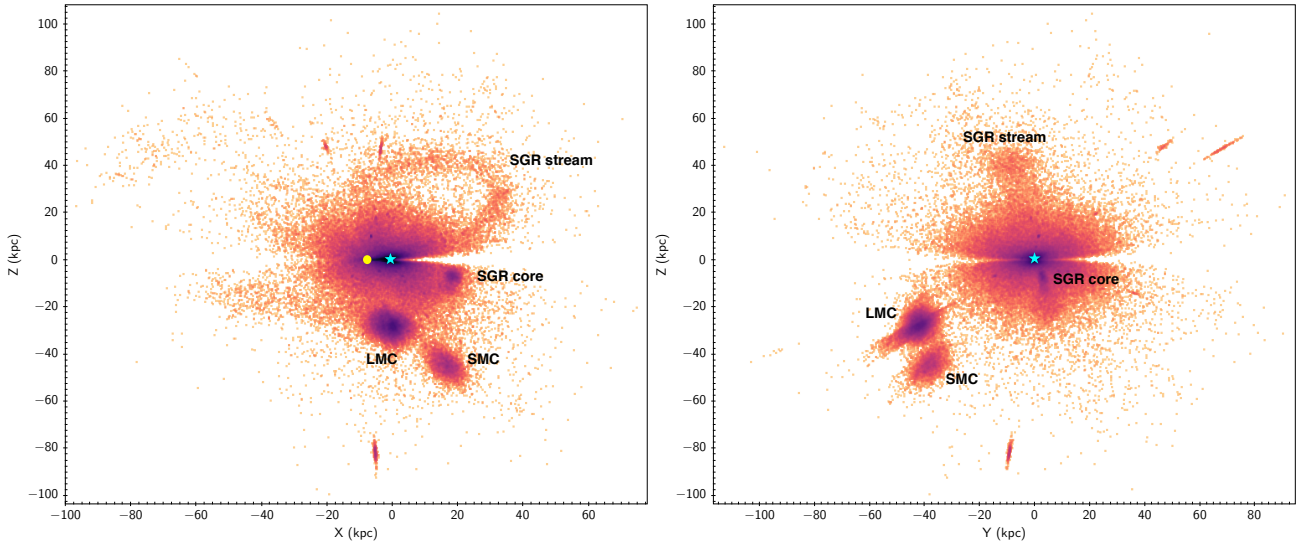


Figure 18. Spatial distribution of RRLs in our sample on the Cartesian X - Z (*left panel*) and Y - Z (*right panel*) planes. The blue star and the yellow circle show the centre of our Galaxy and the Sun, respectively. The LMC, SMC, the Sgr stream and core are clearly seen.

erature that were derived from *Gaia* G -band light curves of RRLs. We found a good agreement (within 0.25 dex) between our values and the metallicity estimates from the literature for most studies. We also analysed the metallicity of RRLs in 38 MW GCs and found that the photometric metallicities of RRLs located in the same cluster have scatter less than 0.3 dex for the majority of GCs, do not show a residual dependence on the period, and that there is consistency

between metallicities of RRab and RRc stars in the same cluster. We provided new estimates of metallicities for the 38 GCs based on their RRLs and found that they are in agreement with the values from Carretta et al. (2009) within the errors.

We used our metallicity measurements to calculate the distances to 134,642 RRLs employing the $M_G - [\text{Fe}/\text{H}]$ relation from Garofalo et al. (2022), which is calibrated on *Gaia* EDR3

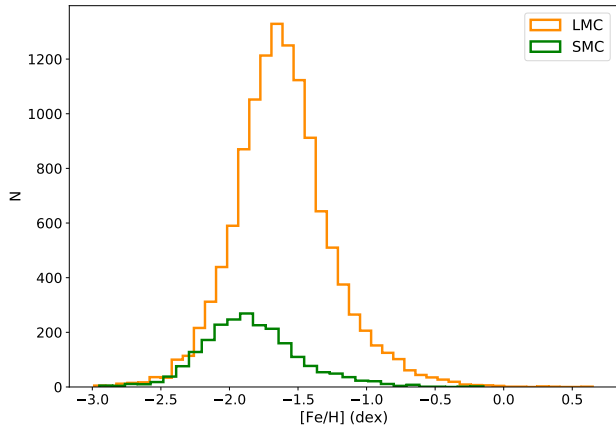


Figure 19. Metallicity distribution of the RRLs in the LMC and SMC.

parallaxes. We used these distances to estimate the mean distances to 38 MW GCs and to map the LMC, the SMC, the Sgr stream and its core as traced by RRLs on the Cartesian coordinates plane. We calculated mean metallicity and distance to the LMC: $[\text{Fe}/\text{H}]_{\text{LMC}} = -1.63 \pm 0.36$ dex and $\mu_{\text{LMC}} = 18.55 \pm 0.18$ mag, and the SMC: $[\text{Fe}/\text{H}]_{\text{SMC}} = -1.86 \pm 0.36$ dex and $\mu_{\text{SMC}} = 19.01 \pm 0.17$ mag, in excellent agreement with previous estimates in the literature. We also confirmed that the RRLs in the north-eastern part of the LMC are closer to us than RRLs in the south-western part (Cusano et al. 2021). Our results show that the catalogue of $\sim 134,000$ RRLs with distances and metallicities provided in this study is a powerful tool to study the structure and chemical abundance of the MW and the Local Group galaxies and to search for the new substructures in our Galaxy and beyond.

ACKNOWLEDGEMENTS

This work uses data from the European Space Agency mission *Gaia* (<https://www.cosmos.esa.int/gaia>), processed by the *Gaia* Data Processing and Analysis Consortium (DPAC; <https://www.cosmos.esa.int/web/gaia/dpac/consortium>). Funding for the DPAC has been provided by national institutions, in particular the institutions participating in the *Gaia* Multilateral Agreement. Support to this study has been provided by INAF Mini-Grant (PI: Tatiana Muraveva), by the Agenzia Spaziale Italiana (ASI) through contract and ASI 2018-24-HH.0, and by Premiale 2015, Mining The Cosmos - Big Data and Innovative Italian Technology for Frontiers Astrophysics and Cosmology (MITiC; P.I.B. Garilli).

DATA AVAILABILITY

The data underlying this article are available in the article and in its online supplementary material.

REFERENCES

- Andrievsky S., et al., 2018, *PASP*, **130**, 024201
- Belokurov V., Deason A. J., Koposov S. E., Catelan M., Erkal D., Drake A. J., Evans N. W., 2018, *MNRAS*, **477**, 1472
- Bono G., Caputo F., Castellani V., Marconi M., Storm J., Degl’Innocenti S., 2003, *MNRAS*, **344**, 1097
- Borissova J., Minniti D., Rejkuba M., Alves D., 2006, *A&A*, **460**, 459
- Carretta E., Bragaglia A., Gratton R., D’Orazi V., Lucatello S., 2009, *A&A*, **508**, 695
- Chadid M., Sneden C., Preston G. W., 2017, *ApJ*, **835**, 187
- Clement C. M., et al., 2001, *AJ*, **122**, 2587
- Clementini G., Carretta E., Gratton R., Merighi R., Mould J. R., McCarthy J. K., 1995, *AJ*, **110**, 2319
- Clementini G., Gratton R., Bragaglia A., Carretta E., Di Fabrizio L., Maio M., 2003, *AJ*, **125**, 1309
- Clementini G., et al., 2019, *A&A*, **622**, A60
- Clementini G., et al., 2023, *A&A*, **674**, A18
- Crestani J., et al., 2021, *ApJ*, **908**, 20
- Cusano F., et al., 2021, *MNRAS*, **504**, 1
- Dékány I., Grebel E. K., 2022, *ApJS*, **261**, 33
- Dékány I., Grebel E. K., Pojmański G., 2021, *ApJ*, **920**, 33
- Drake A. J., et al., 2013, *ApJ*, **763**, 32
- Fernley J., Barnes T. G., 1996, *A&A*, **312**, 957
- For B.-Q., Sneden C., Preston G. W., 2011, *ApJS*, **197**, 29
- Freedman W. L., Madore B. F., Scowcroft V., Burns C., Monson A., Persson S. E., Seibert M., Rigby J., 2012, *ApJ*, **758**, 24
- GRAVITY Collaboration et al., 2018, *A&A*, **615**, L15
- Gaia Collaboration et al., 2016, *A&A*, **595**, A1
- Gaia Collaboration et al., 2021, *A&A*, **649**, A1
- Gaia Collaboration et al., 2023, *A&A*, **674**, A1
- Garofalo A., Tantaló M., Cusano F., Clementini G., Calura F., Muraveva T., Paris D., Speziali R., 2021, *ApJ*, **916**, 10
- Garofalo A., Delgado H. E., Sarro L. M., Clementini G., Muraveva T., Marconi M., Ripepi V., 2022, *MNRAS*, **513**, 788
- Gilligan C. K., et al., 2021, *MNRAS*, **503**, 4719
- Govea J., Gomez T., Preston G. W., Sneden C., 2014, *ApJ*, **782**, 59
- Graczyk D., et al., 2020, *ApJ*, **904**, 13
- Gratton R. G., Bragaglia A., Clementini G., Carretta E., Di Fabrizio L., Maio M., Taribello E., 2004, *A&A*, **421**, 937
- Hajdu G., Dékány I., Catelan M., Grebel E. K., Jurcsik J., 2018, *ApJ*, **857**, 55
- Harris W. E., 2010, *arXiv e-prints*, p. arXiv:1012.3224
- Hoffman M. D., Gelman A., 2011, *arXiv e-prints*, p. arXiv:1111.4246
- Huang Y., et al., 2021, *ApJ*, **907**, 68
- Iorio G., Belokurov V., 2019, *MNRAS*, **482**, 3868
- Iorio G., Belokurov V., 2021, *MNRAS*, **502**, 5686
- Jurcsik J., Kovacs G., 1996, *A&A*, **312**, 111
- Lambert D. L., Heath J. E., Lemke M., Drake J., 1996, *ApJS*, **103**, 183
- Layden A. C., 1994, *AJ*, **108**, 1016
- Li X.-Y., Huang Y., Liu G.-C., Beers T. C., Zhang H.-W., 2023, *ApJ*, **944**, 88
- Liu S., Zhao G., Chen Y.-Q., Takeda Y., Honda S., 2013, *Research in Astronomy and Astrophysics*, **13**, 1307
- Liu G. C., et al., 2020, *ApJS*, **247**, 68
- Longmore A. J., Fernley J. A., Jameson R. F., 1986, *MNRAS*, **220**, 279
- Madore B. F., et al., 2013, *ApJ*, **776**, 135
- Molnár L., Pál A., Plachy E., Ripepi V., Moretti M. I., Szabó R., Kiss L. L., 2015, *ApJ*, **812**, 2
- Morgan S. M., Wahl J. N., Wiecehorst R. M., 2007, *MNRAS*, **374**, 1421
- Mullen J. P., et al., 2021, *ApJ*, **912**, 144
- Muraveva T., et al., 2018a, *MNRAS*, **473**, 3131
- Muraveva T., Garofalo A., Scowcroft V., Clementini G., Freedman W. L., Madore B. F., Monson A. J., 2018b, *MNRAS*, **480**, 4138
- Muraveva T., Delgado H. E., Clementini G., Sarro L. M., Garofalo A., 2018c, *MNRAS*, **481**, 1195
- Muraveva T., Clementini G., Garofalo A., Cusano F., 2020, *MNRAS*, **499**, 4040
- Nemec J. M., Cohen J. G., Ripepi V., Derekas A., Moskalik P., Sesar B., Chadid M., Bruntt H., 2013, *ApJ*, **773**, 181
- Pancino E., Britavskiy N., Romano D., Cacciari C., Mucciarelli A., Clementini G., 2015, *MNRAS*, **447**, 2404
- Pedregosa F., et al., 2011, *Journal of Machine Learning Research*, **12**, 2825
- Pietrzyński G., et al., 2019, *Nature*, **567**, 200
- Plachy E., et al., 2021, *ApJS*, **253**, 11
- Preston G. W., 1959, *ApJ*, **130**, 507
- Schlegel D. J., Finkbeiner D. P., Davis M., 1998, *ApJ*, **500**, 525

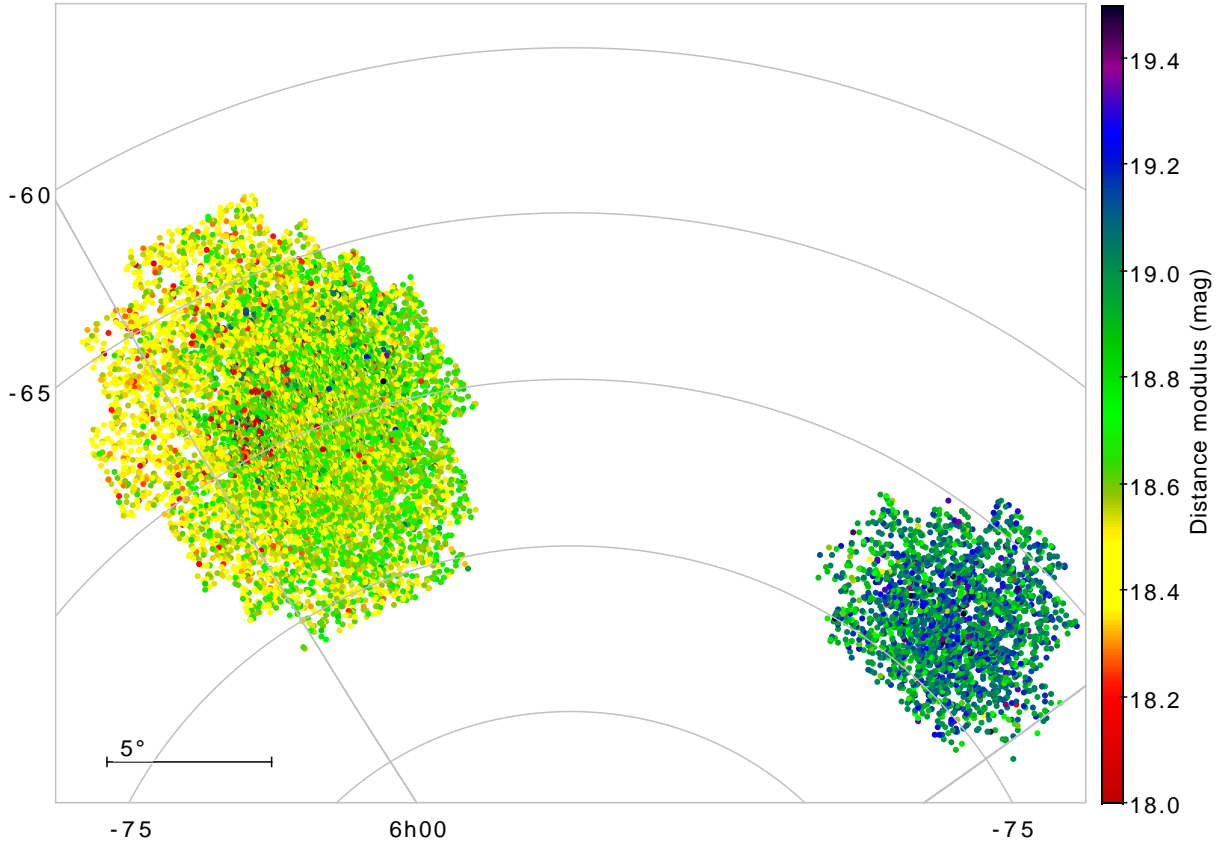


Figure 20. Sky distribution of the RRLs in the LMC and SMC, colour-coded by distance modulus

- Scowcroft V., Freedman W. L., Madore B. F., Monson A., Persson S. E., Rich J., Seibert M., Rigby J. R., 2016, *ApJ*, 816, 49
- Sesar B., et al., 2014, *ApJ*, 793, 135
- Skowron D. M., et al., 2016, *Acta Astron.*, 66, 269
- Skowron D. M., et al., 2021, *ApJS*, 252, 23
- Smolec R., 2005, *Acta Astron.*, 55, 59
- Snedden C., Preston G. W., Chadid M., Adamów M., 2017, *ApJ*, 848, 68
- Sollima A., Cacciari C., Arkharov A. A. H., Larionov V. M., Gorshanov D. L., Efimova N. V., Piersimoni A., 2008, *MNRAS*, 384, 1583
- Soszyński I., et al., 2014, *Acta Astron.*, 64, 177
- Soszyński I., et al., 2019, *Acta Astron.*, 69, 321
- Zinn R., West M. J., 1984, *ApJS*, 55, 45
- Zinn R., Chen X., Layden A. C., Casetti-Dinescu D. I., 2020, *MNRAS*, 492, 2161

APPENDIX A: DATASET

Table A1. Parameters of the 150 RRLs in HR-CAT-RRLS sample: (1) *Gaia* DR3 source_id; (2) and (3) Coordinates; (4) RRL type; (5) Period; (6) Intensity-averaged *G* magnitude; (7)-(11) Fourier parameters; (12) Metallicity from HR-spectroscopy on the metallicity scale adopted by [Crestani et al. \(2021\)](#); (13) Source of metallicity (1 - [Crestani et al. 2021](#), 2 - [For et al. 2011](#), 3 - [Snedden et al. 2017](#), 4 - [Chadid et al. 2017](#), 5 - [Gilligan et al. 2021](#)). Columns (1)-(3) are from *Gaia* DR3 gaia_source table ([Gaia Collaboration et al. 2023](#)). Columns (4)-(11) are from *Gaia* DR3 vari_rr1yrae table ([Clementini et al. 2023](#)).

source_id	RA	DEC	Type	Period	<i>G</i>	A_1	A_2	A_3	ϕ_{21}	ϕ_{31}	[Fe/H]	Source
77849374617106176	30.1396	14.1983	RRab	0.5576	15.67	0.405 ± 0.036	0.167 ± 0.045	–	3.55 ± 0.12	–	-1.78 ± 0.09	1
630421935431871232	151.9310	23.9917	RRab	0.4524	10.65	0.405 ± 0.014	0.177 ± 0.008	0.121 ± 0.012	3.80 ± 0.08	1.64 ± 0.11	-1.58 ± 0.27	1
1191510003353849472	238.3794	12.9611	RRab	0.5221	10.84	0.322 ± 0.005	0.160 ± 0.009	0.085 ± 0.010	4.32 ± 0.05	2.59 ± 0.05	0.05 ± 0.15	4
1234729400256865664	221.8968	16.8453	RRc	0.3149	10.58	0.182 ± 0.004	0.016 ± 0.006	0.014 ± 0.005	4.52 ± 0.28	4.08 ± 0.25	-1.62 ± 0.15	1
1453674738379109760	209.3918	29.8579	RRc	0.3290	11.29	0.181 ± 0.003	0.014 ± 0.004	0.013 ± 0.005	4.82 ± 0.32	4.45 ± 0.25	-1.46 ± 0.15	1
1492230556717187456	214.1524	42.3598	RRc	0.3126	10.91	0.238 ± 0.005	0.075 ± 0.005	0.020 ± 0.004	4.32 ± 0.06	2.37 ± 0.22	-2.54 ± 0.13	1
1565435491138161664	201.5555	56.2570	RRc	0.3071	10.79	0.231 ± 0.003	0.050 ± 0.003	0.014 ± 0.003	4.66 ± 0.06	2.94 ± 0.25	-1.73 ± 0.15	1
1760981190300823808	311.8682	12.4641	RRab	0.4726	9.81	0.227 ± 0.002	0.112 ± 0.002	0.065 ± 0.002	4.27 ± 0.02	2.51 ± 0.04	-0.43 ± 0.17	4
1770039418063209600	323.2143	12.8919	RRab	0.6005	13.91	0.232 ± 0.009	0.101 ± 0.010	0.064 ± 0.008	4.02 ± 0.06	1.97 ± 0.16	-1.68 ± 0.11	1
1786827307055763968	321.7645	18.5992	RRab	0.5472	12.77	0.287 ± 0.015	0.140 ± 0.011	0.097 ± 0.011	3.91 ± 0.09	1.92 ± 0.13	-1.67 ± 0.12	1

The table is published in its entirety as Supporting Information with the electronic version of the article. A portion is shown here for guidance regarding its form and content.

Table A2. Parameters of 134,769 RRLs, for which photometric metallicities were calculated in this study: (1) *Gaia* DR3 source_id; (2) and (3) Coordinates; (4) RRL type; (5) Period; (6)-(10) Fourier parameters; (11) Photometric metallicity on the scale adopted by [Crestani et al. \(2021\)](#); (12) Reddening values compiled as described in Section 5; (13) Distance modulus. Columns (1)-(3) are from *Gaia* DR3 *gaia_source* table ([Gaia Collaboration et al. 2023](#)). Columns (4)-(10) are from *Gaia* DR3 *vari_rrlyrae* table ([Clementini et al. 2023](#)).

source_id	RA	DEC	Type	Period	A_1	A_2	A_3	ϕ_{21}	ϕ_{31}	[Fe/H]	$E(B - V)$	μ
500243431117184	44.6981	1.7456	RRab	0.6231	0.311 ± 0.019	0.155 ± 0.026	0.095 ± 0.019	3.95 ± 0.13	1.89 ± 0.32	-2.05 ± 0.50	0.090 ± 0.002	17.53 ± 0.99
507222753405440	44.6653	1.7894	RRab	0.6089	0.335 ± 0.033	0.190 ± 0.030	0.129 ± 0.020	4.03 ± 0.13	1.93 ± 0.31	-1.93 ± 0.48	0.092 ± 0.003	14.02 ± 0.95
584630948352256	46.3415	1.5420	RRab	0.5555	0.278 ± 0.020	0.137 ± 0.015	0.080 ± 0.018	3.96 ± 0.13	2.31 ± 0.22	-1.28 ± 0.44	0.077 ± 0.001	16.61 ± 0.76
782027645388032	46.6991	2.3039	RRab	0.5583	0.277 ± 0.028	0.154 ± 0.034	0.108 ± 0.038	4.43 ± 0.30	2.38 ± 0.44	-1.23 ± 0.57	0.087 ± 0.009	17.09 ± 0.77
1407379179248512	42.8875	1.8053	RRab	0.5813	0.257 ± 0.017	0.116 ± 0.015	0.105 ± 0.017	4.07 ± 0.16	1.93 ± 0.21	-1.78 ± 0.44	0.058 ± 0.001	16.90 ± 0.91
1514169246023424	42.8608	2.4539	RRab	0.6144	0.295 ± 0.073	0.120 ± 0.087	0.116 ± 0.075	4.15 ± 0.32	1.87 ± 0.49	-2.02 ± 0.63	0.087 ± 0.001	15.13 ± 1.00
1742622850845696	45.2336	2.9300	RRab	0.4565	0.342 ± 0.022	0.148 ± 0.032	0.078 ± 0.020	3.73 ± 0.22	1.87 ± 0.33	-1.15 ± 0.48	0.091 ± 0.003	17.22 ± 0.74
2345017784412032	47.2341	2.9847	RRab	0.6143	0.237 ± 0.013	0.127 ± 0.019	0.087 ± 0.018	4.14 ± 0.14	2.41 ± 0.43	-1.51 ± 0.56	0.124 ± 0.001	16.99 ± 0.84
3070042623687040	50.1084	4.9737	RRab	0.5974	0.220 ± 0.008	0.094 ± 0.009	0.058 ± 0.011	3.97 ± 0.12	2.12 ± 0.20	-1.70 ± 0.42	0.160 ± 0.019	17.48 ± 0.87

The table is published in its entirety as Supporting Information with the electronic version of the article. A portion is shown here for guidance regarding its form and content.

APPENDIX B: XGBOOST ANALYSIS

Our Bayesian analysis of the connection between light curve parameters and the metallicity of RRLs assumes a linear correlation, a simplifying assumption that may not capture more intricate, subtle dependencies within the data. To explore the potential existence of complex and weak relationships, we employed an XGBoost regressor to predict the metallicity using the *Gaia* DR3 data, with the RRab stars in the HR-CAT-RRLS catalogue serving as the training set.

The decision to utilize the XGBoost algorithm was driven by the many advantages it provides for the task we set out to accomplish. The efficiency of XGBoost in handling non-linear relationships, together with its adeptness at handling complex tabular data played a pivotal role in our choice. Another compelling factor in favor of XGBoost is its capacity to deliver exceptionally high performance and robustness, even when confronted with relatively small datasets. XGBoost’s resilience makes it a reliable choice for extracting meaningful insights from the limited observational data available.

Furthermore, the time efficiency of XGBoost is noteworthy. Its capability to complete full training experiments within a limited time frame is advantageous, allowing to allocate more time to fine-tuning the algorithm and augmenting the dataset. This not only enhances the model’s predictive accuracy but also provides an opportunity for a more comprehensive exploration of the parameter space.

Our dataset was randomly split into training and validation sets, with the training set representing 80% of the full catalogue, with the rest being held out as validation set. Before starting the training process, we applied a quantile transformation with uniform output to the data, using all the features of the light curve Fourier decomposition and period. After scaling the data, we expanded the dataset by creating additional columns that quantify the similarity of each input to the average values within specific groups. These groups were defined by segregating the data into bins based on their metallicity values. Each column in this series reflects the degree of resemblance between an input and the average values associated with its respective metallicity bin. In practice, we divided the dataset in ten subsamples based on the sample value in terms of metallicity and computed the average values of the input features per bin. The bins were chosen so that no bin was empty. Then, for each sample, we computed the cosine similarity of the input features to the mean values per metallicity bin, including the result in ten additional feature columns, one per bin, following the idea that similar inputs should lead to similar outputs. During training we also applied sample weighting. The weights correspond to the inverse of the KDE smoothing of the metallicity computed on the training set, with a Gaussian kernel and a bandwidth of 0.2.

Performances were optimized by the GridSearchCV function of the SKLearn package (Pedregosa et al. 2011). We used a threefold cross validation, and optimized the number of estimators, the maximum depth of the trees, the learning rate, the lambda regularization, the subsampling of the training set and the columns used per tree and per level. The best RMSE reached on the validation set is 0.29 dex. The corresponding hyperparameters are given in Table B1.

We repeated all test that were carried out for the Bayesian approach, but we did not find a significant increase in performances, possibly indicating that the relationships between the light curve Fourier parameters, periods and the metallicity are indeed linear. It could also be that the data at our disposal are not sufficient to detect more complex correlations, on the account of the training set being too small. In fact, inspecting the learning curve of the model reveals that the RMSE of the training set flattens to values close to the intrinsic scatter of the relation that we find with our Bayesian approach, while that in the validation set flattens to the higher values reported

Parameter	Value
n_estimators	400
max_depth	3
learning_rate	0.09
lambda	1
subsample	0.6
colsample_bylevel	0.7
colsample_bytree	0.9

Table B1. Hyperparameters of the XGBoost regressor with the best performances reached.

above, suggesting that adding more data may allow the model to refine the learned relations.

This paper has been typeset from a $\text{\TeX}/\text{\LaTeX}$ file prepared by the author.